

TECHNICAL UNIVERSITY OF CRETE

MASTER'S THESIS

A Tomographic Hyperspectral Imaging Method: Application in Quantitative Pathology

Author:

Anastasios
Chatziioannou

Supervising Committee:

Professor Costas Balas
Associate Professor Michail Lagoudakis
Associate Professor Vasileios Samoladas

*A thesis submitted in fulfillment of the requirements
for the degree of Master of Science*

in the

Optoelectronics and Biomedical lab
Electrical and Computers Engineers



June, 2020

TECHNICAL UNIVERSITY OF CRETE

Abstract

Optoelectronics and Biomedical lab
Electrical and Computers Engineers

Master of Science

A Tomographic Hyperspectral Imaging Method: Application in Quantitative Pathology

by Anastasios CHATZIOANNOU

A hyperspectral imager is a device that records spectra in the form of a spectral cube (a set of spectral images). There are four types of imagers: whiskbrooms, pushbrooms, staring and snapshot. Nowadays, the market is ruled by pushbroom hyperspectral imagers that require spatial scanning. Spatial scanning - as a mandatory requirement - greatly complicates the process of spectral cube acquisition and introduces spectral and spatial distortions. Staring imagers, on the other hand, require no spatial scanning, but suffer from poor spectral resolution and low throughput. This motivated us to build our own staring-type Hyperspectral Imager. The goal was to build a device that requires no spatial scanning and outputs clear spectral images and narrow spectral bands. In this thesis we will uncover how - for the first time - a tomographic spectral cube reconstruction procedure was implemented on a hyperspectral imager. Tomography has never been used in the past in hyperspectral imaging. A separate goal was to design our imager in a way that can be easily adapted on top of digital microscopes. This thesis will explain how a raw spectral cube can be reconstructed to provide high-fidelity spectral cubes with very high spatial resolutions (≥ 6 MP) and very high spectral resolution (wavelength errors ≤ 1 nm). This reconstruction procedure involves our own novel Tomographic Reconstruction algorithm that utilizes the whole spectral cube to output the spectrum of every single pixel. We essentially acquire 6 million spectra per band - for 121 bands - a total of 726 million high-fidelity spectra per cube. Our device finds countless uses in GIS, the food and pharmaceutical industries, but our applications are mainly focused in life-saving solutions, like Quantitative Pathology, where multiple stains may be applied simultaneously on top of blood samples and then separated via spectral unmixing.

Acknowledgements

First and foremost, I would like to thank my parents for their love and countless support for all these years. I would also like to thank my closest friends for supporting me through everything.

This project would not be completed without the assistance of A. Tsapras and C. Rossos. My project advisor, A. Tsapras, tirelessly helped me conduct all the necessary experiments, while C. Rossos, a genius in light sources and hardware, assisted me in handling lasers and LEDs and constructing devices from scratch.

Last but not least, I would like to thank my professor, supervisor and mentor, Dr. Costas Balas for guiding and trusting me the past 3 years, during my 1 year thesis and 2 years M.Sc. studies.

Contents

1	Hyperspectral Imaging	1
1.1	The evolution of spectroscopy	1
1.2	Spectral imaging in our everyday life	2
1.3	The physics behind spectral imaging	4
1.4	Multi vs Hyper spectral imaging	6
1.5	Hyperspectral imaging devices	6
1.5.1	Spatial scanning	7
1.5.2	Non-scanning (Snapshot Spectral Imaging)	9
1.5.3	Spectral scanning	11
1.5.4	Spatio-spectral scanning	12
1.6	Optical filters	12
1.6.1	Optical filtering	12
	Central Wavelength	12
	Bandwidth (Full Width Half Max)	12
	Blocking range	13
	Slope	14
	Optical Density	14
	Dichroic Filter	15
	Cut-On/Cut-off Wavelength	15
1.6.2	Fixed filters	16
	Optical Filter Fabrication Techniques	16
	Absorptive and Dichroic Filters	17
	Exploring Dichroic Bandpass Filters	18
	Linear Variable Bandpass Filters	19
1.6.3	Tunable filters	20

	Fabry–Pérot Interferometers	20
	Liquid Crystal Tunable Filters	20
	Acousto-optic Tunable Filters	21
1.7	Applications in non destructive analysis	23
1.8	Applications of Hyperspectral Imaging in medicine	24
1.8.1	Absorption Hyperspectral Microscopy	24
1.8.2	Fluorescence Hyperspectral Microscopy	26
1.9	Applications of Hyperspectral Imaging in medicine: Useful tools and methods	27
1.9.1	Microscopy	27
1.9.2	Spectral Similarity Mapping: Application in Histology	28
1.9.3	Spectral Deconvolution: Application in Histology	30
1.9.4	Classification: Focus on biomedical imaging	32
	Support Vector Machines	32
	Artificial neural networks	33
	Spectral angle mapper	33
2	Tomographic Reconstruction	35
2.1	Raw cube acquisition	35
2.2	The non-uniformity problem	36
2.3	Spectral deviation	37
2.4	Spectro-spatial mapping	41
2.5	Tomographic cube reconstruction	43
2.5.1	The downside of the tomographic method	44
2.5.2	Enhancement by linear interpolation	44
2.5.3	Improvements to the linear interpolation assisted tomography Improvements in the spectral domain	46
	Improvements in the temporal domain	48
2.5.4	Validation of tomographic method with interpolation	48
	Gray values vs RGB	48
	Minimum requirements	49
	Margin of error	50

Results of reconstruction	50
3 Hardware	53
3.1 Muses9-HS	53
3.1.1 Muses9-HS: Linear variable optical filter	55
3.1.2 Muses9-HS: CMOS Sensor	57
3.1.3 Motorized system	59
4 Software	61
4.1 Muses9 Spectral Suite	61
4.1.1 Modes of operation	61
Spectral Imaging	62
Spectral Cube Acquisition	63
4.1.2 Spectral cube analysis	64
4.1.3 Calibrating the device	65
5 Quantitative Pathology	69
5.1 Morphometry	69
5.1.1 Group Morphometry	70
5.1.2 Diagnostic Morphometry	70
5.2 Cytometry	71
5.2.1 Static cytometry	71
5.2.2 Flow cytometry	71
5.2.3 Cytophotometry	73
5.2.4 Laserscan microscopy	73
5.2.5 Image cytometry	73
5.3 Hyperspectral Imaging	74
6 Conclusions	77
Bibliography	79

List of Figures

1.1	Inside a spectroscope.	2
1.2	Human eye's spectral response.	3
1.3	RGB camera spectral response (Sony IMX178).	3
1.4	The RGB Bayer filter.	4
1.5	Absorbance.	5
1.6	HSI categories	7
1.7	Spatial scanning: Push-broom HSI design	7
1.8	Spatial scanning: a) whisk-broom, b) push-broom	8
1.9	Spatial scanning: Inside a push-broom HSI	9
1.10	Snapshot Spectral Imaging: Mosaic	10
1.11	Snapshot Spectral Imaging: Tiled	10
1.12	Illustration of Center Wavelength and Full Width at Half Maximum	13
1.13	Illustration of Blocking Range	14
1.14	Illustration of Optical Density	15
1.15	Illustration of a Dichroic Filter Coating	15
1.16	Illustration of Cut-On Wavelength	16
1.17	Illustration of Cut-Off Wavelength	16
1.18	Deposition of Multiple Layers of alternating High and Low Index Materials onto a Glass Substrate	18
1.19	Linear Variable Filters	19
1.20	Liquid Crystal Tunable Filters	20
1.21	Liquid Crystal Tunable Filter transmission	21
1.22	Acousto-Optic Tunable Filter	22
1.23	Acousto-Optic Tunable Filter transmission	22
1.24	Restoring El Greco's St Francis of Assisi.	23

1.25 Reading underneath the manuscript using IR imaging.	24
1.26 Seeing beneath the painting.	24
1.27 Distinguishing lymphocytes from lymphoblasts	25
1.28 The concentration maps of FR (a) and HEM (b). The pseudocolor scale ranges from black to white as the concentration varies from zero to maximum.	26
1.29 Fluorescence: Detecting Circulating Tumor Cells.	26
1.30 Microscope schematics.	28
1.31 Spectral similarity mapping in action. (a) original; (b) selected regions from original and their spectra which act as references; (c), (d) and (e) show the regions emphasized where the three selected spectra most closely match.	29
1.32 Absorption spectrum of a mixture of A and B (thick line). The decon- volution process 'tries' a range of scaling values for A and B spectra until the best fit is obtained to the actual data. In the example shown this corresponds to around 50% of A and 75% of B. 'Percent' in this case is relative to the reference spectra.	30
2.1 Linear variable optical filter.	35
2.2 Linear variable optical filter with a motor.	36
2.3 Acquired "raw" spectral image on 590nm.	37
2.4 Standard deviation (σ_λ) of a spectral image's frequencies.	38
2.5 Spectral cube of a white target (450-700nm)	38
2.6 Sampling the spectral images.	39
2.7 Cube fragments - Filter linearity	39
2.8 Filter linearity - Unique RGBs.	40
2.9 Calculating spectral deviations.	41
2.10 Map of pixel to wavelength correlation.	42
2.11 Illustration of the tomographic reconstruction.	43
2.12 Tomographic reconstruction: stripe effect.	44
2.13 Spectrum: Requested and Actual wavelengths.	45
2.14 Linear interpolation on the shifted spectrum.	46

2.15 RGB camera spectral response (Sony IMX178).	49
2.16 Acquired RGB spectral cube.	51
2.17 Reconstructed RGB spectral cube.	51
2.18 590nm reconstructed.	52
3.1 Muses9-HS1700	53
3.2 Linear Variable Filter.	55
3.3 Linear Variable Filter response.	55
3.4 Linear Variable Filter blocking ability.	56
3.5 QHY5-III-178	58
3.6 QHY5-III-178 readout noise.	59
3.7 The Arduino Nano.	59
3.8 The Trinamic Stepper Motor.	60
4.1 Software: Modes of operation	61
4.2 Software: Spectral imaging	62
4.3 Software: Spectral cube acquisition	63
4.4 Software: Viewing spectral cubes	64
4.5 Software: Clustering with k-Means	65
4.6 Sony IMX178M (Monochrome) Quantum Efficiency (QE)	66
4.7 Linear Variable Filter response.	66
4.8 Software: Calibrating the device	67

List of Abbreviations

HS	Hyper Spectral
MS	Multi Spectral
HSI	Hyper Spectral Imager
HSI	Hyper Spectral Imaging
FPI	Fabry P�erot Interferometers
RGB	Red Green Blue
LVF	Linear Variable Filter
LCTF	Liquid Crystal Tunable Filter

Chapter 1

Hyperspectral Imaging

1.1 The evolution of spectroscopy

Spectroscopy is the science of analyzing light from a whole spectrum to narrow bands. Spectroscopy is rich in spectral information, but lacks spatial information, as it involves the collection of spectral data from a single point. In hyperspectral imaging a N -pixel image contains N spectra, analyzed to narrow bands. In that sense, hyperspectral imaging is superior to spectroscopy, as the one dimensional space of spectroscopy evolves to a three dimensional cube of spectral and spatial information.

A spectroscope or spectrometer is a device that receives the incoming radiation (light) through a tiny slit of 1-2mm height and $5\text{-}800\mu\text{m}$ width. The light is then analyzed using a prism and focused using a lens onto a light sensor. The sensor can be a photographic plate, CCD or CMOS array. These devices collect photons and convert them to electrical signals. A full spectrum can be reconstructed in real time based on the amount of collected photons and the physical location of the sensor's photon collectors.

The small size of the slit greatly enhances the precision in point spectroscopy, but also greatly reduces the throughput of the incoming radiation. This means that a large amount of light (photons) is required for the device to operate in real time. This problem is solved by either boosting the light source (if possible) or increasing the integration time of the CCD array. In hyperspectral imaging there is no such problem, as the incoming light is collected through a lens, without a slit.

The spectrometer is a very useful device that cannot be fully replaced by an HSI

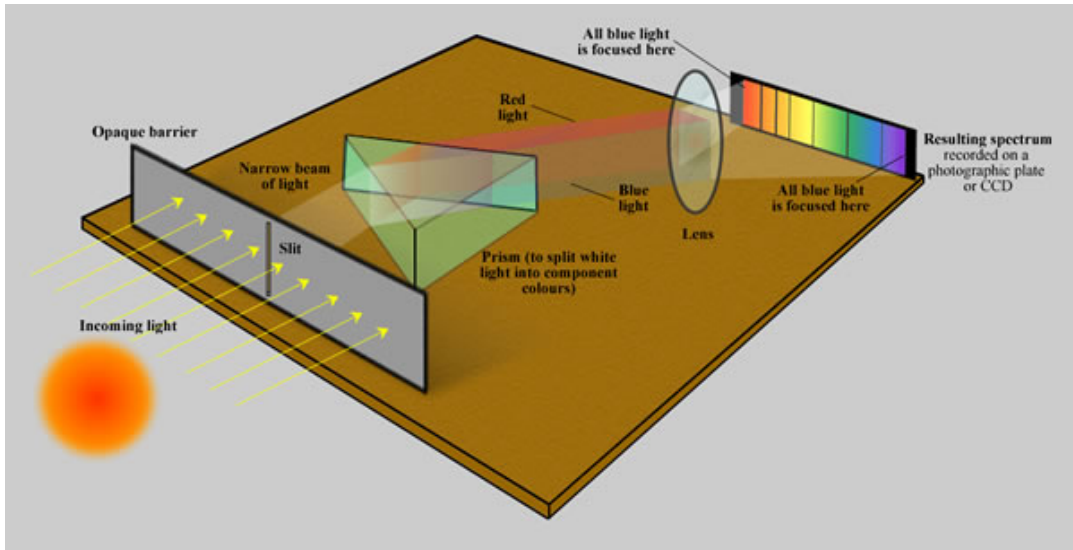


FIGURE 1.1: Inside a spectroscope.

(HyperSpectral Imager), as it can generate a full spectrum in a split millisecond. However, HSIs are the product of the evolution of spectroscopy, since they can capture millions of spectra from a target; the spectrometer can only capture a single spectrum.

1.2 Spectral imaging in our everyday life

Human eyes have evolved to perceive different frequencies of the incoming visible radiation as color. To fully describe a color, only three components are required, the levels of red, green and blue radiation. This model was created in accordance to the human eye's receptors. The human eye has evolved to separate these three components, in order to perceive threats, distinguish between various chemical elements and scan the environment. This is a perfect example of a multispectral imager. The visible radiation 400-700nm enters through the eye's pupil and triggers three types of electrical signals, as shown in figure 1.2.

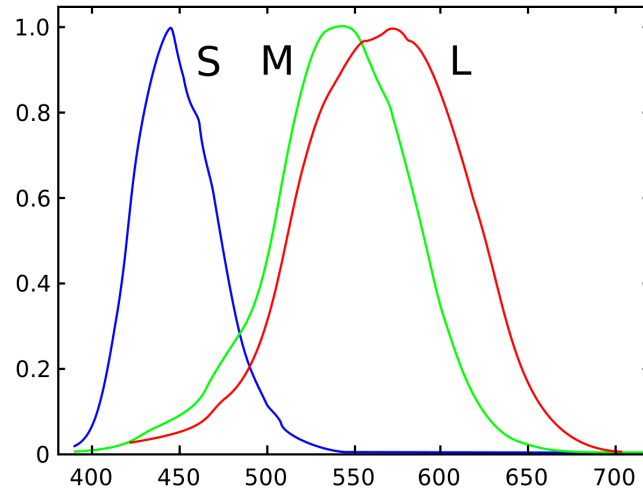


FIGURE 1.2: Human eye's spectral response.

The most common RGB cameras (e.g. smartphone cameras) mimic the eye's spectral response (see Fig. 1.3). They use three (3) wide, usually overlapping filters that allow only certain frequencies to enter, while reflecting the rest of the visible frequencies. A common N -pixel RGB camera is made of $4 * N$ MOSFETs, on top of which is placed a Bayer filter.

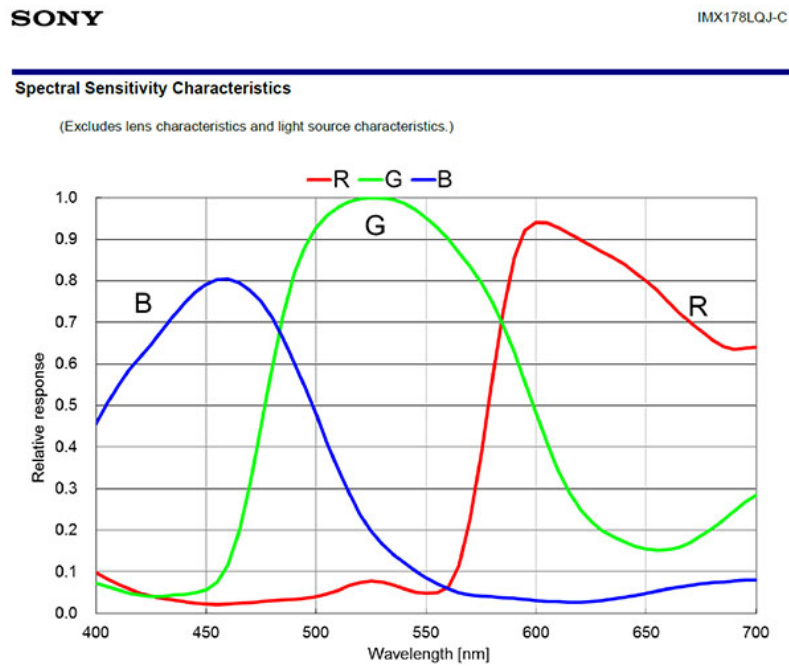


FIGURE 1.3: RGB camera spectral response (Sony IMX178).

The Bayer filter is a mosaic of red, green and blue optical band-pass filters that allow only their respective frequencies (see Fig. 1.3). A Bayer filter places 4 optical filters on top of each pixel, which is made of 4 MOSFET (CMOS) transistors, 2 green,

1 red, 1 blue (see Fig. 1.4). The second green was used to mimic the physiology of the eye, as the human eye is more perceptive near the middle of the visible spectrum (green colored frequencies). The Bayer filter can be modified to use RGBIR filters, switching a green filter with an IR optical filter, expanding the observable spectrum. The Bayer filter's mask size can also be modified to 8, 16, 32, ... in order to fit more optical filters in each pixel, essentially trading spatial resolution for spectral resolution.

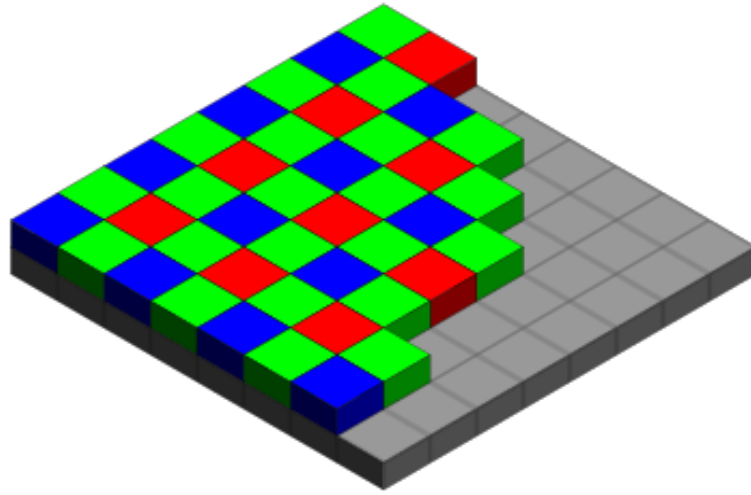


FIGURE 1.4: The RGB Bayer filter.

1.3 The physics behind spectral imaging

In a spectrophotometer, light over a range of wavelengths is shone through a sample and the amount of light transmitted through the sample is measured. The quantity 'absorbance' (often referred to as 'optical density') is determined and Beer's law is applied: this states that, for randomly distributed absorbers or chromophores, light absorption at a particular wavelength is proportional to the concentration (C) of the absorbing medium and the thickness (d) of the sample.

$$A_{(\lambda)} = \epsilon_{(\lambda)} \times C \times d$$

ϵ is known as the extinction coefficient at the particular wavelength λ used for the measurement.

The relationship between the light transmittance (T) through the sample and the optical density (absorbance), again at a specific wavelength, is given by Lambert's law:

$$T_{(\lambda)} = \frac{I_{transmitted(\lambda)}}{I_{incident(\lambda)}}$$

The combination is generally known as the Beer-Lambert law:

$$\log_{10}\left[\frac{I_{incident(\lambda)}}{I_{transmitted(\lambda)}}\right] = -\log_{10}T_{(\lambda)} = \epsilon_{(\lambda)} \times C \times d$$

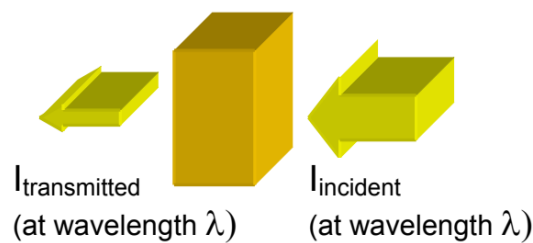


FIGURE 1.5: Absorbance.

The measurement of $A_{(\lambda)}$ gives an absolute measurement of the transparency (or opacity) of the medium with respect to the wavelength. This opacity is related to the amount of material present in the sample. If this material had an absorption at only one wavelength, then we would need to perform the measurement only at that wavelength. Moreover, the sample would appear transparent at all other wavelengths. However, almost all chemical materials absorb a range of wavelengths (i.e. there are different extinction coefficients at different wavelengths). This gives rise to an absorption spectrum, a kind of fingerprint or signature for that material. If the extinction coefficients at the different wavelengths are known (as is often the case for chemical samples dissolved in liquids, i.e. measured in a spectrophotometer cell), then again, we could choose a single wavelength at which to do the experiment to determine the concentration or amount of material present. *Spectral imaging applied to histology*

1.4 Multi vs Hyper spectral imaging

In order to easily separate the two main categories of spectral imaging, one may consider multispectral imaging as a discrete sampling procedure, and hyperspectral imaging as continuous.

Multispectral imagery typically refers to 3 to 10 bands. Multispectral cubes are smaller in size and may or may not consist of wider bands.

Hyperspectral imagery, on the other hand, consists of more than 10 bands, with a width of about 1-10nm each. A hyperspectral cube may have even narrower or wider bands, as there is no definite rule that separates a multispectral from a hyperspectral cube. An HS (HyperSpectral) cube may possess more than 100 bands, e.g. a full VIS-IR spectrum cube (400-1000nm) with 5nm precision consists of 121 narrow bands.

Ultraspectral refers to an even finer spectral resolution, that usually has a very small spatial resolution, of just a few pixels.

1.5 Hyperspectral imaging devices

A hyperspectral imager (HSI) is a device that collects spectral and spatial information in the form of an array of images. We refer to an array of spectral images as a Hyper-Spectral Cube. A device that captures an HS cube is called a Hyper-Spectral Imager (HSI). There are four basic types of HSIs, and each type extends to smaller subcategories.

The four basic types of HSIs are:

- Spatial scanning
- **Spectral scanning**
- Non-scanning
- Spatio-spectral scanning



FIGURE 1.6: HSI categories

This thesis will cover the **spectral scanning** category. This category was selected because it possesses some advantages that are optimal in our work-cases. The advantages will be explained in detail in 1.5.3.

1.5.1 Spatial scanning

In spatial scanning (see Fig. 1.9), light enters through a long and narrow slit. The slit's dimensions are determined by the manufacturer, but its width cannot surpass 2mm without losing a significant amount of spatial resolution. The scene is projected through this slit onto a diffraction grating that will analyze the light to its spectrum onto the sensor (CMOS, CCD or others).

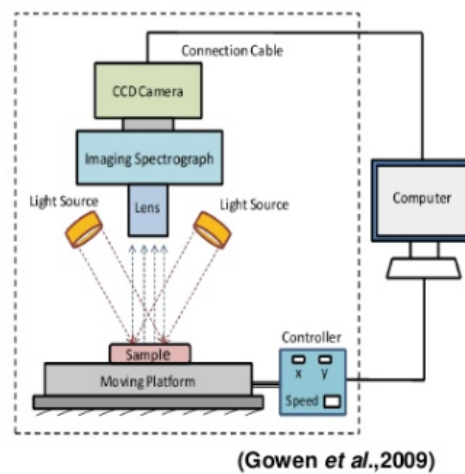


FIGURE 1.7: Spatial scanning: Push-broom HSI design

There are two main types of spatial scanning:

- Whisk-broom scanners
- Push-broom scanners

The **whisk-broom scanners** - resembling the motion of a whisk broom - will move their focus pixel by pixel until the full scene is scanned. These moving parts are expensive and hard to maintain, and so whisk broom type HSIs are not being developed nowadays.

The whisk-broom scanners have been fully replaced throughout the market by their spatial scanning counterparts, the **push-broom scanner**. The push-broom scanner scans a full row instead of a single pixel - resembling the motion of a push broom - "sweeping forward" until the full scene is scanned. The common scanner/photocopier is a push-broom scanning device that contains 1-3 bands; a single band for black and white, or three bands for RGB colored images. Pushbroom HSIs work under the same principle, with the exception that they use a diffraction grating to analyze the light to a maximum of N bands, where N = sensor's height in pixels.

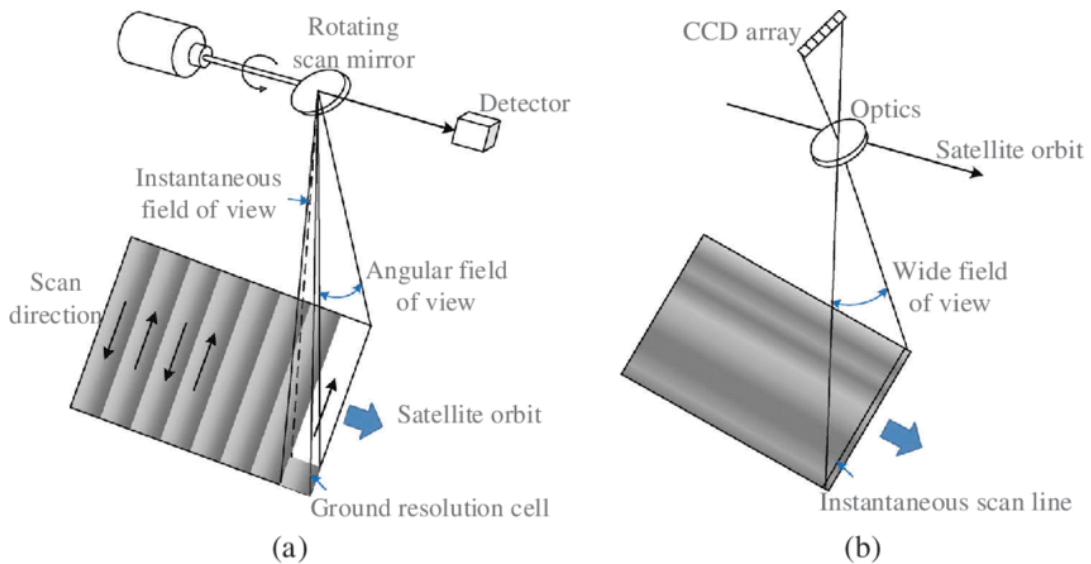


FIGURE 1.8: Spatial scanning: a) whisk-broom, b) push-broom

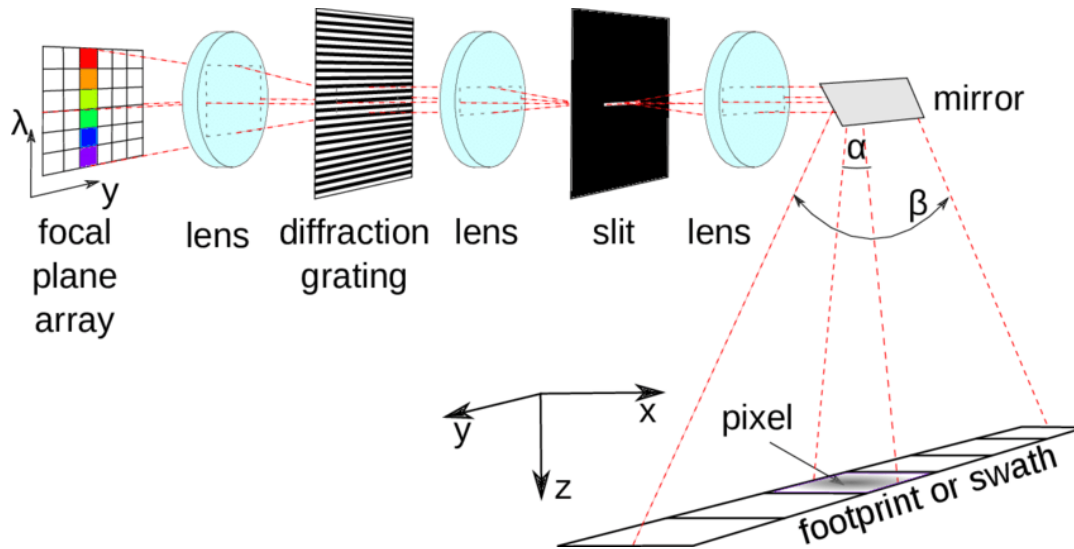


FIGURE 1.9: Spatial scanning: Inside a push-broom HSI

Advantages of a push-broom HSI:

- Few moving parts means low maintenance cost. One may choose to move either the whole HSI, or just the stage (scene).
- Ideal for conveyor belt scanning. The stage moves by itself, and the HSI can be fixed onto a static position.

Disadvantages of a push-broom HSI:

- Smile and keystone distortions (spatial and spectral distortions)
- Push-broom HSIs that use a small stage with a conveyor belt cannot scan large or heavy objects (e.g. art)

1.5.2 Non-scanning (Snapshot Spectral Imaging)

The second most common type of spectral imagers in today's market are snapshot spectral imagers. Snapshot spectral imagers do not involve any type of scanning, as they provide all spectral and spatial information in real time. This type of spectral imagery is crucial in applications where scanning is not an option, because the scene is dynamic (objects in scene either move or change over time).

Even though snapshot imagers provide spatio-spectral information very fast, they will necessarily sacrifice spatio-spectral resolution. Depending on the application, the developer / consumer may choose to prioritize spectral over spatial resolution or vice-versa.

There are two ways to build a snapshot HSI.

The first way is to mimic the Bayer filter and create a custom mosaic of $N \times N$ filters, $N > 2$. These filters can be either fixed (as seen in Fig. 1.10) or tunable (e.g. electro-tunable FPIs). This method will provide realtime spectral information, while sacrificing a lot of spatial resolution.

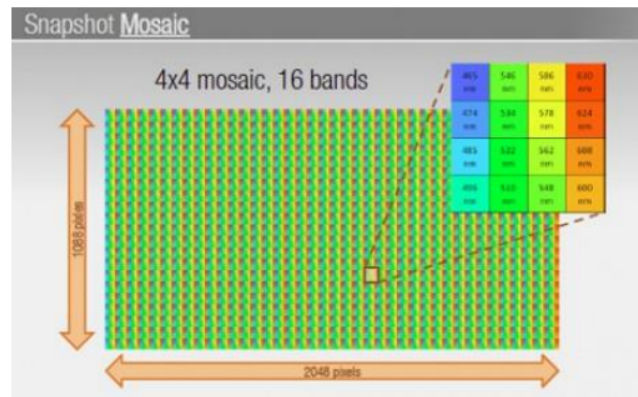


FIGURE 1.10: Snapshot Spectral Imaging: Mosaic

The second way is to create blocks of fixed filters (tiles). This method is not ideal, as every tile observes a different part of the scene. Consequently, either the device or the scene should be moved in order to acquire all spectra, effectively transforming the device from snapshot to spatio-spectral scanning. This reduces the tiled snapshot HSI's applications to a very small number.



FIGURE 1.11: Snapshot Spectral Imaging: Tiled

1.5.3 Spectral scanning

A **spectral scanner** scan a whole scene one wavelength at a time. Light enters through a lens and passes through a tunable filter. The tunable filter will allow a certain band of wavelength(s) to pass and the detector will capture any photons that were not absorbed/reflected.

The tunable filter is chosen by the manufacturer and may be selected based on the application (see 1.6).

Most spectral scanners can display a single band of the full scene real time. This makes them especially useful in certain applications, where the user needs high spectral and spatial resolution in real time (e.g. art restoration). Only snapshot spectral imagers can replicate the same effects, with 2-5x lower spatial resolution.

Even though spectral scanners are, in some cases, a one-way solution, they are useless in dynamic scenes (scenes where the objects move over time). This is the main reason why push-broom and snapshot HSIs have ruled over the market.

The speed of the scanning procedure is determined based on the spectral resolution, and is theoretically completely unaffected by the spatial resolution. This means that preselecting a smaller ROI will not affect the scanning time, but preselecting a smaller amount of bands (selection is always application dependent) can significantly reduce scanning times.

This thesis concerns the construction and improvement of our own spectrum-scanning HSI. Spectral scanning was chosen against other categories, as some of its advantages over other types of HSIs are essential in certain applications, and have not yet been sufficiently explored by other researchers.

Advantages of spectral-scanning:

- Very high spatial resolution
- Realtime display of the whole scene (single band only)
- High spectral fidelity
- Tunable spectral resolution

Disadvantages of spectral-scanning:

- Projected objects must remain unmoved and unchanged (static scene)
- High scanning times for a full HS cube
- Cropping (preselecting smaller ROI) the scene does not affect scanning times

1.5.4 Spatio-spectral scanning

Advanced spatio-spectral scanning systems can be obtained by placing a dispersive element before a spatial scanning system. Scanning can be achieved by moving the whole system relative to the scene, by moving the camera alone, or by moving the slit alone. Spatio-spectral scanning unites some advantages of spatial and spectral scanning, thereby alleviating some of their disadvantages.

1.6 Optical filters

An optical filter selectively transmits one portion of the optical spectrum, while rejecting other portions. They are commonly used in microscopy, spectroscopy, chemical analysis, and machine vision.

1.6.1 Optical filtering

Central Wavelength

Center Wavelength (CWL), used in defining bandpass filters, describes the midpoint of spectral bandwidth over which the filter transmits. Traditional Coated Optical Filters tend to achieve a maximum transmission near the center wavelength, whereas Hard Coated Optical Filters tend to have a fairly flat transmission profile over the spectral bandwidth.

Bandwidth (Full Width Half Max)

Bandwidth is a wavelength range used to denote a specific part of the spectrum that passes incident energy through a filter. Bandwidth is also referred to as FWHM. Full Width-Half Maximum (FWHM) describes the spectral bandwidth over which a

bandpass filter will transmit. The upper and lower limit of that bandwidth is defined at the wavelengths where the filter achieves 50% of the maximum transmission. For example, if the maximum transmission of the filter is 90%, the wavelengths at which the filter achieves 45% transmission will define the upper and lower limits of the FWHM. FWHM's of 10nm or less are considered narrowband and often used for laser clean-up and chemical detection. FWHM's of 25–50nm are often used in machine vision applications; FWHM's of more than 50nm are considered broadband and typically used in fluorescence microscopy applications.

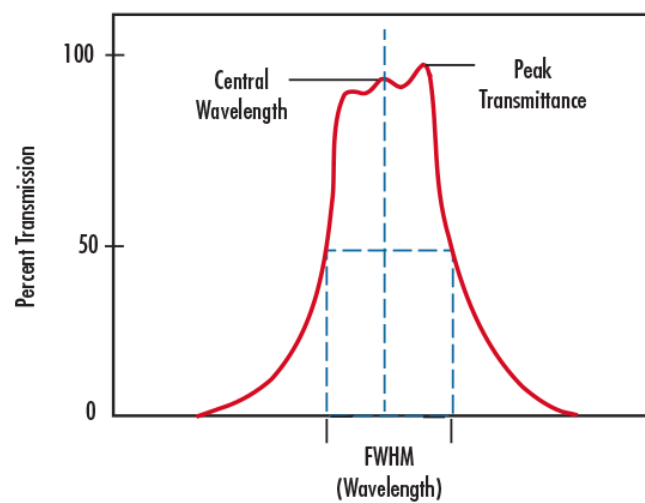


FIGURE 1.12: Illustration of Center Wavelength and Full Width at Half Maximum

Blocking range

Blocking Range is a wavelength interval used to denote a spectral region of energy that is attenuated by the filter (Figure 2). The degree of its blocking is typically specified in terms of optical density.

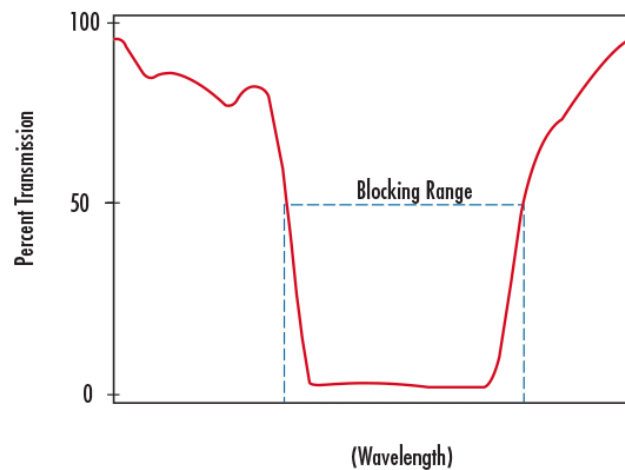


FIGURE 1.13: Illustration of Blocking Range

Slope

Slope is a specification often defined on edge filters, such as shortpass or longpass filters, to describe the bandwidth over which the filter transitions from high blocking to high transmission. Given as the percent of the cut-wavelength, slope can be specified from a variety of starting and end points. Edmund Optics typically specifies the slope as the distance from the 10% transmission point to the 80% transmission point. For example, a 500nm longpass filter with a 1% slope would be expected to transition from 10% transmission to 80% transmission over a 5nm (1% of 500nm) bandwidth.

Optical Density

Optical Density (OD) describes the amount of energy blocked or rejected by a filter. A high optical density value indicates low transmission, and low optical density indicates high transmission. Optical densities of 6 or greater are used for extreme blocking needs such as Raman spectroscopy or fluorescence microscopy. Optical densities of 3.0 – 4.0 are ideal for laser separation and clean-up, machine vision, and chemical detection, while optical densities of 2.0 or less are ideal for color sorting and separating spectral orders.

$$\text{PercentTransmission} = T = 10^{-OD} * 100\%$$

$$OD = -\log\left(\frac{T}{100\%}\right)$$

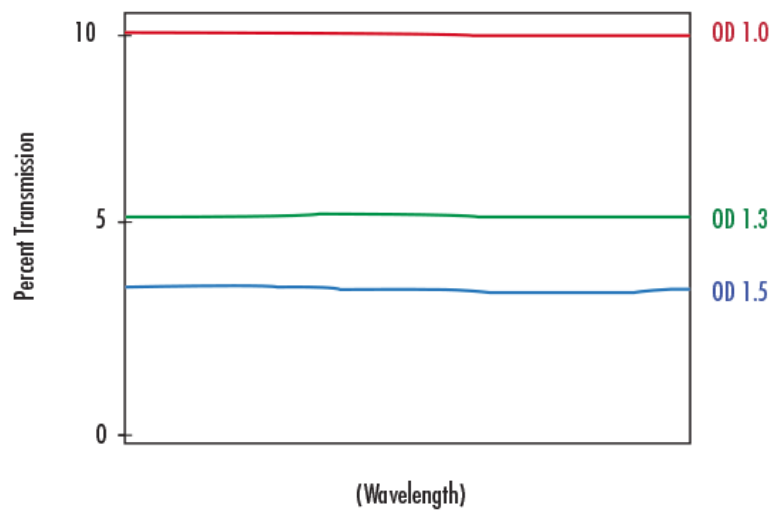


FIGURE 1.14: Illustration of Optical Density

Dichroic Filter

A Dichroic Filter is a type of filter used to transmit or reflect light, depending on the wavelength; light of a specific wavelength range is transmitted, while light of a different range is reflected or absorbed. Dichroic filters are commonly used for longpass and shortpass applications.

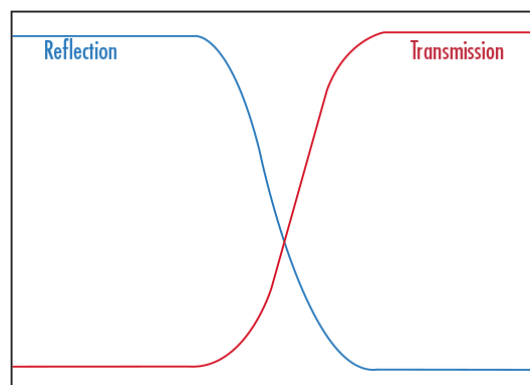


FIGURE 1.15: Illustration of a Dichroic Filter Coating

Cut-On/Cut-off Wavelength

Cut-On Wavelength is a term used to denote the wavelength at which the transmission increases to 50% throughput in a longpass filter. Cut-on wavelength is indicated

by λ_{cut-on} in the figure below.

Cut-Off Wavelength is a term used to denote the wavelength at which the transmission decreases to 50% throughput in a shortpass filter. Cut-off wavelength is indicated by $\lambda_{cut-off}$ in the figure below.[*Optical Filters by EdmundOptics*]

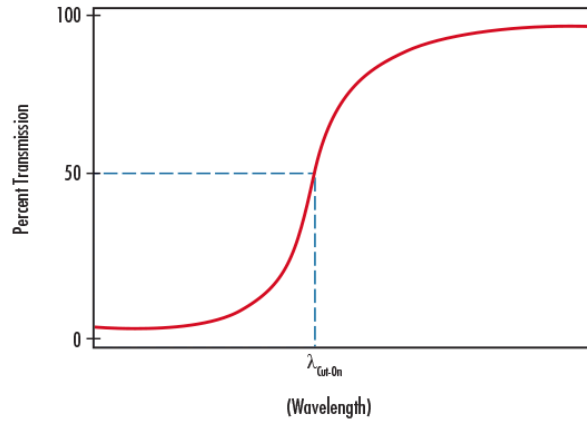


FIGURE 1.16: Illustration of Cut-On Wavelength

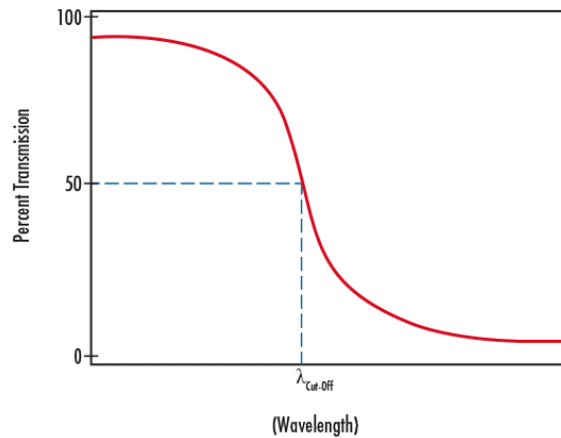


FIGURE 1.17: Illustration of Cut-Off Wavelength

1.6.2 Fixed filters

Optical Filter Fabrication Techniques

In general, filters either absorb unwanted light through the addition of colored glasses or dyes, or reflect unwanted light through the addition of interference coatings. Most EO filters operate on the principal of interference coatings, with coating designs and materials specially selected to achieve the desired transmission shape and performance. Hard Coated Optical Filters feature a single substrate with dense coatings

and excellent optical performance. Designed to meet the adhesion, abrasion, temperature, and humidity requirements specified in MIL-C-48497A, they are ideal for precision requirements and OEM integration. Traditional Coated Optical Filters are typically a stack of absorbing materials, interference coatings, and metallic layers, laminated together to create a low-cost, efficient filter. The complexity of the assembly, however, limits both the optical performance and environmental stability of such filters. Nonetheless, traditional coated filters are ideal for laboratory equipment and analytical instrumentation. Colored Glass Filters and other absorbing filters like Plastic Filters and Wratten Filters, introduce elements, compounds, dyes, or other colorants to a base substrate to manipulate the filter's spectral properties. The resulting filters are relatively inexpensive, but have less desirable optical properties than similar coated filters. Absorptive filters are typically integrated into illumination and sensing applications. [*Optical Filters by EdmundOptics*]

Absorptive and Dichroic Filters

The wide range of optical filters can be broken into two main categories: absorptive and dichroic. The difference between the two does not lie in what they filter, but how they filter. In an absorptive filter, light is blocked based on the absorption properties of the glass substrate used. In other words, light that is blocked does not reflect off the filter; rather, it is absorbed and contained within the filter. In applications where noise in a system from unwanted light is an issue, an absorptive filter is ideal. Absorptive filters also have the added bonus of not being very angle sensitive; light can be incident upon the filter from a wide range of angles and the filter will maintain its transmission and absorption properties.

Conversely, a dichroic filter works by reflecting unwanted wavelengths, while transmitting the desired portion of the spectrum. In some applications, this is a desirable effect because light can be separated by wavelength into two sources. This is achieved by adding a layer, or multiple layers, of material of varying indexes of refraction to exploit the interference nature of light waves. In interference filters, light traveling from a lower index material will reflect off a higher index material; only light of a certain angle and wavelength will constructively interfere with the

incoming beam and pass through the material, while all other light will destructively interfere and reflect off the material.

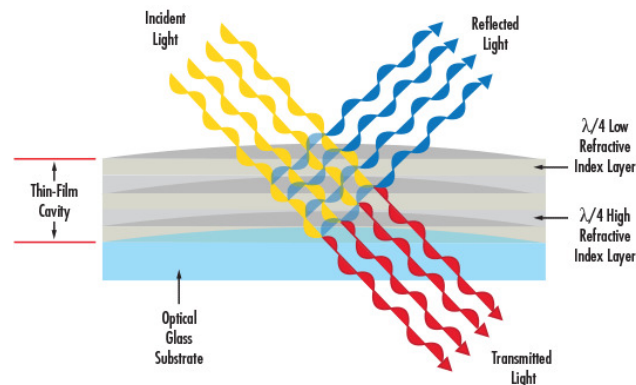


FIGURE 1.18: Deposition of Multiple Layers of alternating High and Low Index Materials onto a Glass Substrate

Unlike absorptive filters, dichroic filters are extremely angle sensitive. When used for any angle(s) outside of their intended design, dichroic filters cannot meet the transmission and wavelength specifications originally indicated. As a rule of thumb, increasing the angle of incidence through a dichroic filter will shift it towards shorter wavelengths (i.e. towards bluer wavelengths); and decreasing the angle will shift it towards longer wavelengths (i.e. towards redder wavelengths). [*Optical Filters by EdmundOptics*]

Exploring Dichroic Bandpass Filters

Bandpass filters are used in a wide range of industries and can be either dichroic or color substrate. Dichroic bandpass filters are manufactured by two different techniques: traditional and hard sputtered, or hard coated. Both techniques achieve their unique transmission and reflection properties by a deposition of numerous layers of alternating high and low index of refraction materials onto glass substrates. In fact, depending upon the application, there can be more than 100 layers of material deposited per face of a given substrate.

The difference between traditional-coated filters and hard-sputtered filters is the number of substrate layers. In traditional-coated bandpass filters, layers of varying index materials are deposited onto multiple substrates which are then sandwiched together. For example, imagine the illustration in Figure 7 repeated up to and even

more than 100 times. This technique leads to a thick filter with reduced transmission. This reduction in transmission is caused by incident light traveling through and being absorbed and/or reflected by numerous substrate layers. Conversely, in hard-sputtered bandpass filters, materials of varying indices are deposited onto only a single substrate (Figure 8). This technique leads to thin filters with high transmission. For additional information on fabrication techniques, view [An Introduction to Optical Coatings](#). View the [Benefits of Hard Coatings](#) to help you select the correct filter for your application. [[Optical Filters by EdmundOptics](#)]

Linear Variable Bandpass Filters

Linear Variable Bandpass Filters are precision coated optical filters with spectral properties that vary linearly across the length of the filter. Linear Variable Bandpass Filters feature high transmission across narrow bandwidths along with deep blocking of unwanted light to maximize system performance at the required wavelength. Spectral response can be adjusted simply by moving the filter's position relative to the light source. Additionally, a single Linear Variable Bandpass Filter can replace multiple dedicated filters to simplify system setup and minimize weight. [[Optical Filters by EdmundOptics](#)]

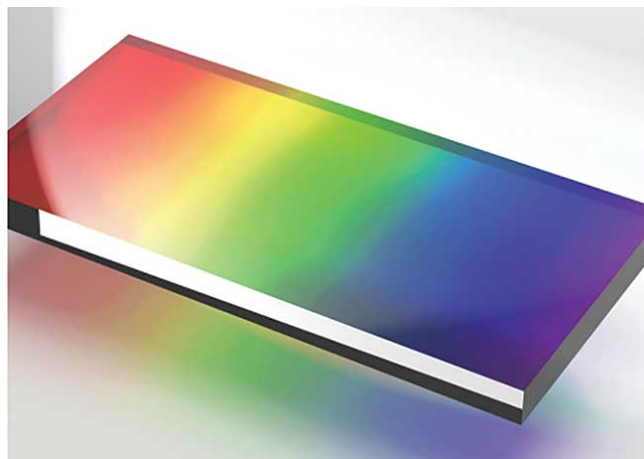


FIGURE 1.19: Linear Variable Filters

1.6.3 Tunable filters

Fabry–Pérot Interferometers

A variation of dichroic filters are **etalons** or **Fabry–Pérot interferometers** (FPI). An optical wave may pass through the optical cavity of an FPI only if they are in resonance. FPIs make use of the interference phenomenon to discard any wavelengths that do not resonate to it. Recent progress in technology has made etalons tunable and the size of a CMOS. Etalons are being used on top of pixels or in front of the detector, allowing for either spectral scanning or snapshot imagery.

Liquid Crystal Tunable Filters

Another type of tunable filters are **liquid crystal tunable filters** (LCTFs). It is a Lyot-Ohman filter with many stages, each comprising: one solid (fixed) and one liquid (variable) birefringent crystal, sandwiched between two cross polarizers. Each stage has different variable retardance and produce a sinusoidal transmittance pattern with different peak wavelength, defined by constructive interference conditions. All combined transmittances give a single band, which is tunable through voltage control.

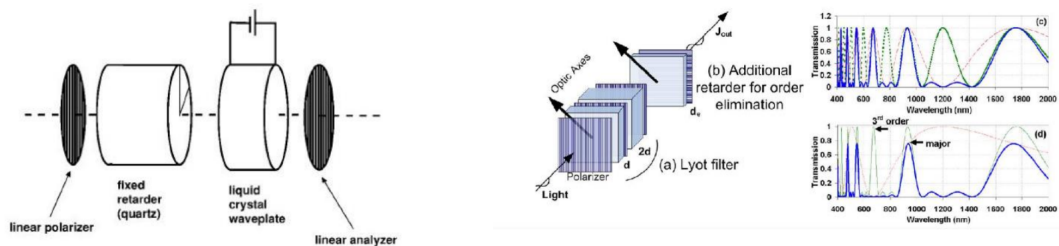


FIGURE 1.20: Liquid Crystal Tunable Filters

Advantages:

- No moving parts
- Can be miniaturized
- Fast switching (50ms)

Disadvantages:

- Poor and variable transmittance (50% of 60%= 30% max)

- Broad band
- Limited range (one octave/unit)
- Liquid crystals can be used destroyed if a high power source is used

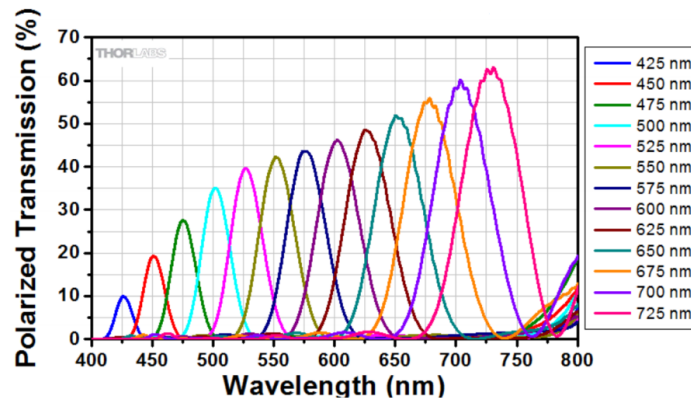


FIGURE 1.21: Liquid Crystal Tunable Filter transmission

Acousto-optic Tunable Filters

Acousto-optic tunable filters are based on the diffraction of light from a volume grating formed by acoustic shear waves (RF) traveling in a single crystal of a material like tellurium dioxide (TeO_2). The central, 0-order undiffracted beam and one of the polarized diffracted beams are blocked, and the second polarized diffracted beam is used. This line is tuned by the RF.

Advantages:

- No moving parts
- Narrow band
- Can be used with lasers
- Very fast switching (<1ms)

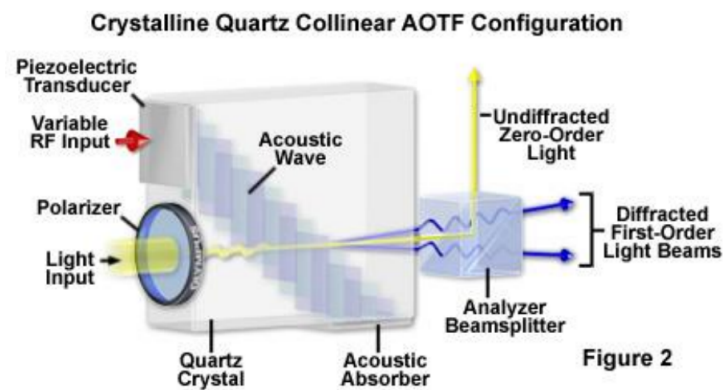


FIGURE 1.22: Acousto-Optic Tunable Filter

Disadvantages:

- Poor (polarization) but flat transmittance
- Poor out of band blocking
- Very small aperture
- High power consumption

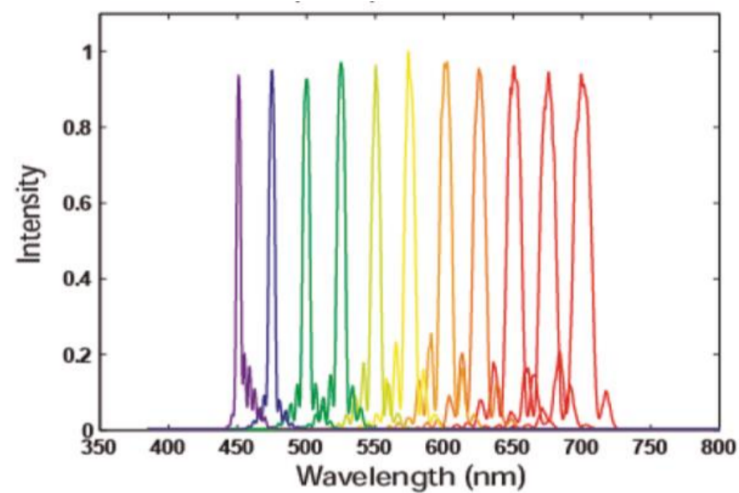


FIGURE 1.23: Acousto-Optic Tunable Filter transmission

1.7 Applications in non destructive analysis

When analyzing specimen from artwork or other ancient artifacts, they must be handled with utmost care. Destructive methods involve removal of precious material for lab microanalysis. They include optical microscopy, scanning electron microscopy, micro-Fourier transform infrared spectroscopy (l-FTIR), micro-Raman spectroscopy, high-pressure liquid chromatography (HPLC), gas chromatography, and others. **Non destructive methods** exploit light matter interaction in non visible bands. They present however a trade-off between spatial and spectral (analytical) information. These include infrared reflectography, thermography, X-ray techniques, point spectroscopies, multi-and hyperspectral imaging.

Employing non destructive methods of scientific analysis of paintings is essential, as we may:

- Reveal hidden information beneath the painting.
- Authenticate and detect forgeries.
- Document and categorize artwork.
- Preserve by detecting deterioration marks.
- Restore deterioration with ease using an HSI.

Using a spectral-scanning HSI or a snapshot spectral imager and a UVA lamp, we take advantage of the fluorescence to reveal any intervention (Balas et al., 2018).



El Greco *St Francis of Assisi*

Multimodal operation



Fluorescence spectral imaging revealing intervention

FIGURE 1.24: Restoring El Greco's St Francis of Assisi.

Using IR and SWIR (Short-Wave Infrared) HSIs we can read erased manuscripts. This feature is also applicable in forensics and forgery detection.

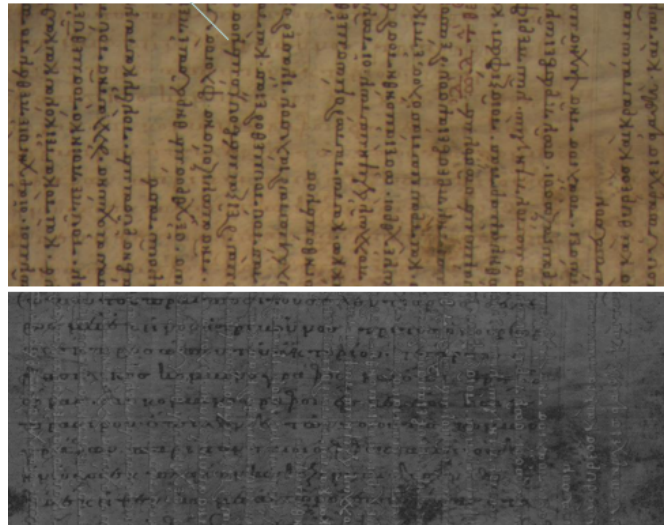


FIGURE 1.25: Reading underneath the manuscript using IR imaging.

Using IR and SWIR imaging we may also reveal a whole picture, invisible to the naked eye, either due to deterioration and decay, or due to repainting.

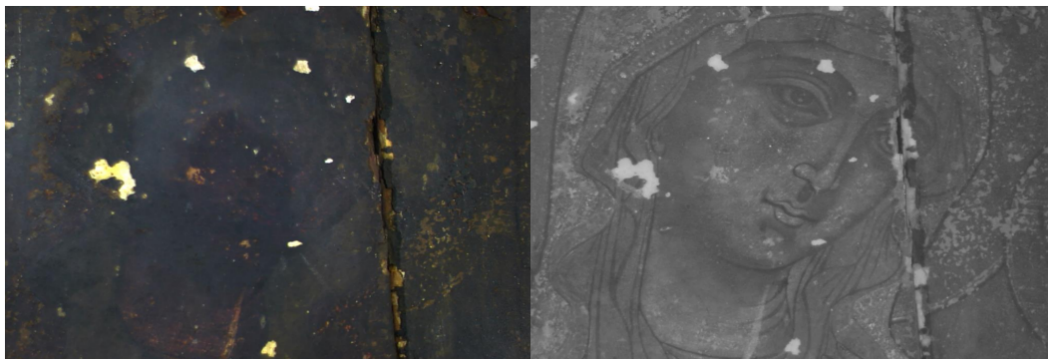


FIGURE 1.26: Seeing beneath the painting.

1.8 Applications of Hyperspectral Imaging in medicine

1.8.1 Absorption Hyperspectral Microscopy

In histology, tissue samples examined with absorption hyperspectral microscopy may provide accurate diagnosis (Balas, 2019).

The first case we will explore is **Acute Lymphoblastic Leukemia (ALL)**. ALL is a malignant disorder of the blood. Accurate diagnosis is essential for disease

management and follow up. The routine procedure is employing two staining solutions, May-Grunwald (MG) and Giemsa (G). These stain blood samples and aid in the detection and differentiation of normal blood cells vs leukemic cells. ALL comprises 75% of all acute leukemia cases. With early diagnosis, it is the most successfully treated type of childhood leukemia. Lymphoblasts in peripheral blood circulation are similar morphologically to lymphocytes. They are, however, quite distinguishable when analyzing their spectra.

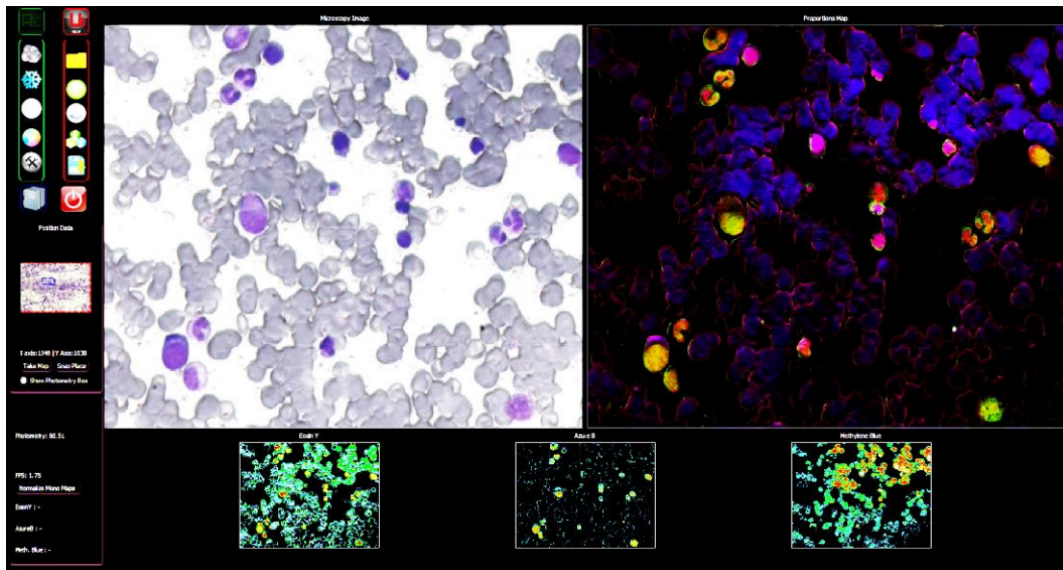


FIGURE 1.27: Distinguishing lymphocytes from lymphoblasts

The second case we will explore is managing cancer using stain concentration mapping (Balas, 2019). Decision making for chemotherapy and/or endocrine therapy is largely based on estrogen and progesterone receptors expression by the breast cancer cells. The routine procedures use suitable monoclonal antibodies against ERs and PgRs recognizing the cellular antigen (ERs, PRs). The product is a red precipitate azo dye ($C_{26}H_{23}ClN_3O_2$) (chromagen Fast Red (FR)). Non stained areas are counterstained with Hematoxylin (HEM) ($C_{16}H_{14}O_6$). FR and HEM spectra substantially overlap. Quantitative assessment of relative concentrations is impossible with conventional methods. In Hyperspectral imaging, however, we may separate the added solutions through spectral unmixing.

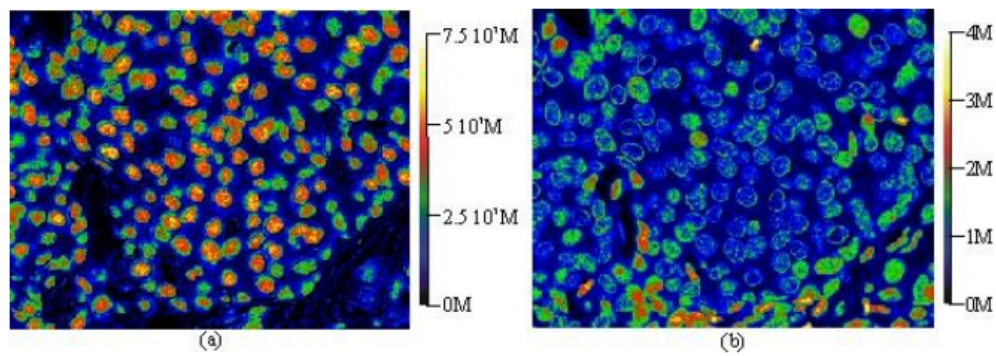


FIGURE 1.28: The concentration maps of FR (a) and HEM (b). The pseudocolor scale ranges from black to white as the concentration varies from zero to maximum.

1.8.2 Fluorescence Hyperspectral Microscopy

Fluorescence aids in precise cancer profiling for personalizing medicine, by detecting **Circulating Tumor Cells** (Balas, 2019). By detecting, enumerating and profiling tumor cells in blood circulation, we may define the risk of metastases and generate a chemotherapy or immunotherapy strategy / model (type and brand of medicine, dosage, risks).



FIGURE 1.29: Fluorescence: Detecting Circulating Tumor Cells.

1.9 Applications of Hyperspectral Imaging in medicine: Useful tools and methods

Hyperspectral imaging is a relatively new science that is still being researched / developed. The applications in everyday life, research and industry are numerous and keep increasing.

1.9.1 Microscopy

Spectral imaging in medicine is especially useful when combined with microscopy.

Transmitted light microscopy (bright-field microscopy) is the most commonly used method in the examination of histological samples, i.e. tissue sections stained with one or more dyes or stains, more generally called chromophores. These chromophores have been developed and perfected over many decades, are universally used in the field, and in general are optimised to stain subcellular features of 'thin' tissue sections. The expression of a particular chromophore is very much a function of the particular protocol used in the preparation of the slide.

Direct visual observation is clearly the simplest and to a large extent the most versatile technique but is limited in the ability to quantify the resulting images. The human eye-brain combination is an excellent sensor for observing and identifying particular morphological features but is extremely limited in its ability to quantify these features, either in terms of morphology areas or in terms of distributions of 'amounts' of material present in a particular area. Most 'measures' have thus been limited to the adoption of some arbitrary scale (e.g. high, medium, low) or to some form of counting (e.g. cell nuclei observed at high magnifying power).

The combination of an electronic imager (i.e. camera) with an image processing device (i.e. computer) forms a tool which is very good at quantifying features but is generally limited in its ability to recognise features of interest, particularly when several such features are partially or wholly superimposed. The use of a spectrally-resolved imager is an attempt at enhancing the ability of an electronic device to 'segment' or delineate wanted features. *Spectral imaging applied to histology*

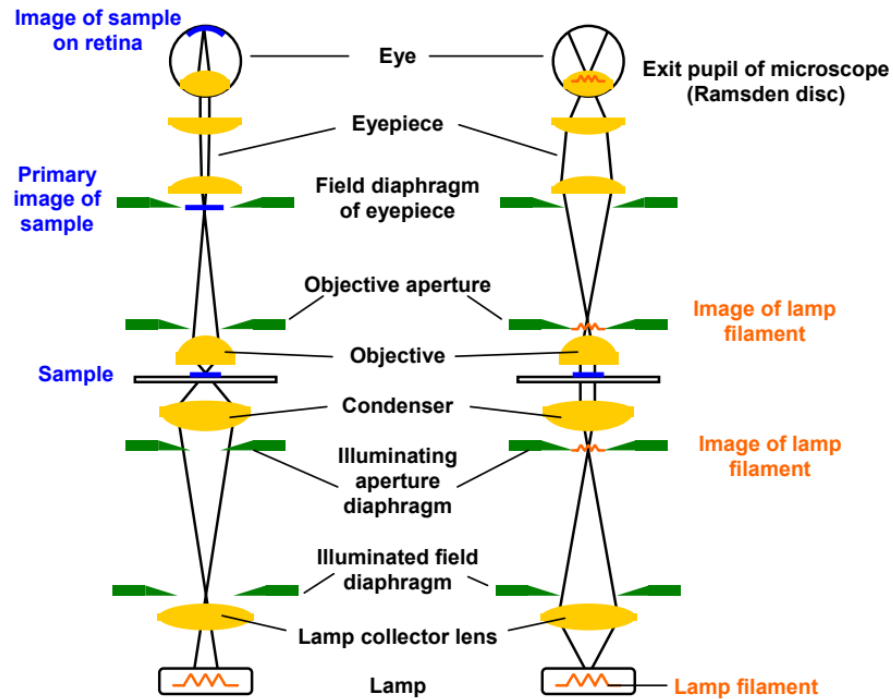


FIGURE 1.30: Microscope schematics.

1.9.2 Spectral Similarity Mapping: Application in Histology

Spectral Similarity Mapping (SSM) is a convenient method which is applicable when we are not really interested in determining the contributions that each chromophore makes to the overall spectrum determined at each pixel, but rather when we wish to identify all the regions of the image, i.e. all the pixels that have a similar absorption spectrum. In other words, we wish to identify the parts of the section that have a similar staining intensity but are not necessarily concerned about what biology/biochemistry has caused the staining.

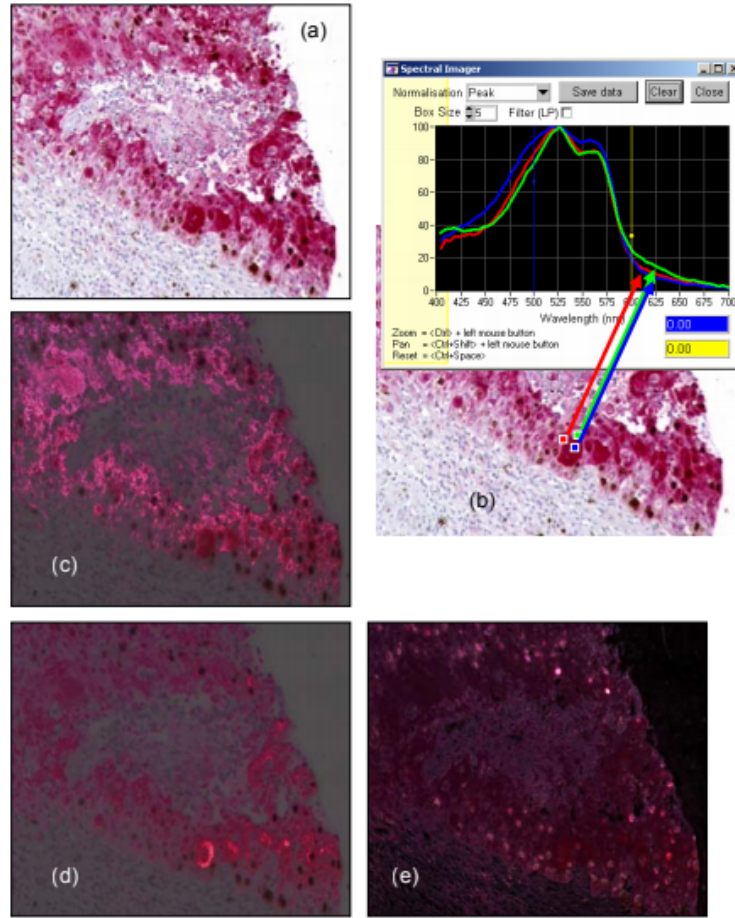


FIGURE 1.31: Spectral similarity mapping in action. (a) original; (b) selected regions from original and their spectra which act as references; (c), (d) and (e) show the regions emphasized where the three selected spectra most closely match.

Clearly we need to define a reference (i.e. reference spectrum) with which to compare all the pixels in the image. The result of doing this on 3 separate regions of a slide is shown in Fig. 1.31. The software compares the spectrum at every pixel with that taken from the reference region(s). The more similar they are, the greater the brightness value assigned to that pixel and hence 'similar' regions become apparent. But of course there must be some formalised way of defining this similarity. The comparison is performed mathematically by defining the spectral difference between the wanted (reference) spectrum and the actual spectrum at every pixel. This is performed in a 'weighted' fashion as shown in the equation below, where I_0 is the reference spectrum and I is the pixel spectrum:

$$\text{SpectralDifference} = \left(\int_{\lambda_1}^{\lambda_2} [I_{x,y}(\lambda) - I_0(\lambda)]^2 d\lambda \right)^{1/2}$$

In this example, a metastatic squamous cell carcinoma has been labelled with pi-monidazole (pink/red regions) and Ki-67 (brown regions). In panel (d) blood vessels have been segmented reasonably successfully, even though the differences between spectra are small, and certainly hard to see by eye. *Spectral imaging applied to histology*

1.9.3 Spectral Deconvolution: Application in Histology

Spectral Deconvolution (SD) or decomposition is most useful when we suspect (as is often the case) that spectral absorption contributions from more than one chromophore are present in some or each of the pixels. This process starts with a set of reference spectra for the chromophores in question. These spectra can be obtained from the sample itself if there regions which are deemed to be singly-stained. Alternatively (and more commonly applicable), accurate spectra of individual dyes can be obtained from singly-stained slides. The best fit to the actual spectrum is then obtained by varying the ‘proportions’ of A and B reference spectra. This process is shown in Fig. 1.32

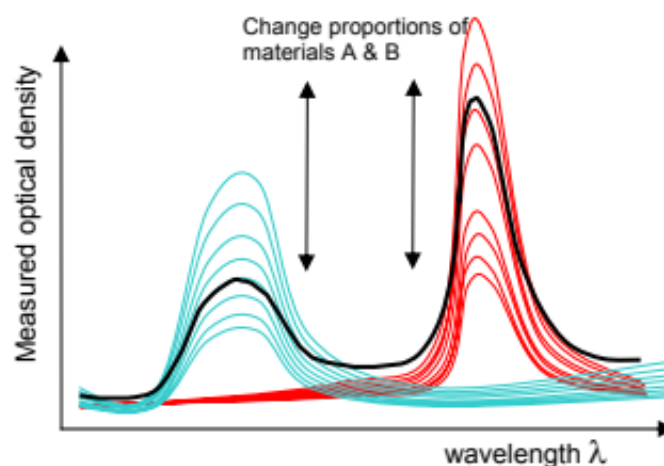


FIGURE 1.32: Absorption spectrum of a mixture of A and B (thick line). The deconvolution process ‘tries’ a range of scaling values for A and B spectra until the best fit is obtained to the actual data. In the example shown this corresponds to around 50% of A and 75% of B. ‘Percent’ in this case is relative to the reference spectra.

Each of the reference spectra can be thought of as representing an amount or concentration of a particular chromophore. While we do not know the actual value of concentration (because we do not know extinction coefficients nor path lengths), we

can express the concentration or amount in every pixel of our sample as a percentage in relation to the reference spectrum. In other words, if the software finds, as in the above example, that, at a given pixel, A's spectrum needs to be reduced by scaling to 1/2 its reference spectrum amplitude, and B's spectrum needs to be reduced by scaling to 3/4 its reference spectrum amplitude in order to obtain a good fit to the actual spectrum, it is acceptable to conclude one of the following:

- If the tissue thicknesses used are the same in the reference and sample slides, then A's staining intensity is half that present in A's reference slide and B's staining intensity is 3/4 of that present in its reference slide.
- If the tissue thicknesses are not the same, then an appropriate correction must be made. For example, if A's reference slide was twice as thick as the sample slide, then the sample and reference actually contain the same concentration of material.
- If we find, at some other pixel, that A's contribution has dropped to 1/4, then that pixel can be said to contain 1/2 the amount of material compared to the first pixel.

Similarly, it is NOT correct to conclude that A and B are present in sample in the ratio of concentrations of 1:1.5 (i.e. 1/2 : 3/4) for the pixel data presented in the example. This would only be true if we were able to develop some standardised method of defining reference slides where different stains could be arranged to be present at the same concentration.

From the above, it should be reasonably obvious that relationships between staining intensities of the SAME chromophore, at different pixels in a given image can be safely derived (assuming that the tissue section is consistently flat over the imaged area. It also means that different regions (i.e. images) from the SAME slide can be similarly inter-compared. Relationships between DIFFERENT chromophores on the SAME slide can also be safely made but NOT on any kind of absolute scale.

A slightly trickier problem is inter-comparison of the SAME chromophore on DIFFERENT slides. This is fine if the slides are from the same batch/staining run, and of course if they are of identical thickness. It is clear that caution must be applied

if slides from different batches/staining runs are compared. Even with a high degree of quality control, it is well known that minor differences are often inevitable. This will create a systematic error between batches but could in principle be corrected for if at least two similar (adjacent) sections are used, one in each batch. *Spectral imaging applied to histology*

1.9.4 Classification: Focus on biomedical imaging

Hyperspectral image classification methods applied in the medical area mainly include pixel and subpixel classification based on the type of pixel information used. Pixel-wise classification can be parametric or nonparametric. Parametric classifiers generally assume normal distribution for the data, which is often violated in practice. Nonparametric methods, such as support vector machines (SVMs) and artificial neural networks (ANN) are widely used in medical hyperspectral image processing. The subpixel method assumes the spectral value of each pixel to be a linear or nonlinear combination of pure components. Pixel- and subpixel-based methods can be supervised or unsupervised. Commonly used supervised classification methods include SVMs, ANN, spectral information divergence (SID), and spectral angle mapper (SAM). [Lu and Fei, 2014]

Support Vector Machines

SVM is a kernel-based machine learning technique that has been widely used in the classification of hyperspectral images. Due to its strong theoretical foundation, good generalization capability, low sensitivity to the curse of dimensionality, and ability to find global classification solutions, SVM is usually preferred by many researchers over other classification paradigms.

SVM has been proved to perform well for classifying hyperspectral data. In the processing of medical hyperspectral data, SVM has also been explored for various classification tasks. Melgani and Bruzzone [Melgani and Bruzzone, 2004] investigated the effectiveness of SVMs in the classification of hyperspectral remote sensing data. It was found that SVMs were much more effective than radial-basis function (RBF) neural networks and the K-nearest neighbor classifier in terms of classification accuracy, computational time, and stability to parameter settings. Kong et al.

[Kong, 2005] chose Gaussian RBF kernel as the kernel function for SVM and learned the SVM parameters from 100 training samples chosen randomly from each of the normal and tumor classes. For testing, 2036 (normal) and 517 (tumor) samples were used. Experimental results showed that the spatial filtering enhanced the performance, which resulted in an overall accuracy of 86%, while the use of the original data had an accuracy of 83%.

Artificial neural networks

Neural network is another supervised classification method that has been adopted by many researchers, due to its nonparametric nature, arbitrary decision boundary, etc. Multilayer perceptron (MLP) is the most popular type of neural network in image classification. It is a feed-forward network trained by the backpropagation algorithm. Monteiro et al. [Monteiro, 2004] implemented both single-layer perceptron (SLP) and MLP as supervised classifiers. The MLP notably generated the clearest visualization of the calendar's number under the blood. Although the SLP was also able to learn a good visualization, the output presented more noise.

Spectral angle mapper

SAM determines the spectral similarity by calculating the angle between the spectra and treating them as vectors in a space with dimensionality equal to the number of wavelengths. Martin et al. [Martin, Thies, and Gerstner, 2012] employed SAM algorithm to map the spectral similarity between image spectra and cluster spectra in order to perform supervised classification, and they found that SAM disregarded specific surface irregularities of the vocal cords that naturally led to inhomogeneous reflections in every patient. Li et al. [Li, 2012] used the SAM algorithm to identify the nerve fibers from the molecular hyperspectral images of nerve sections according to the difference of the spectral signatures of different parts.

Chapter 2

Tomographic Reconstruction

2.1 Raw cube acquisition

As stated earlier, throughout the entirety of our experiments, the Hyperspectral Imager (HSI) we will use is our own staring type **HSI**, Muses9-HS1700. This imager features a linear variable optical filter (see Fig. 2.1) in the 400-1000 range to separate wavelengths and a CMOS monochromatic (or RGB bayer filtered) sensor to capture the photons. The linear filter is placed between the lens and the sensor. In order to acquire a specific band from our specimen and/or scene, the linear filter must be placed in the exact location that separates the requested wavelength. This is an automated procedure that uses a stepper motor to physically move the linear filter along its X-axis.

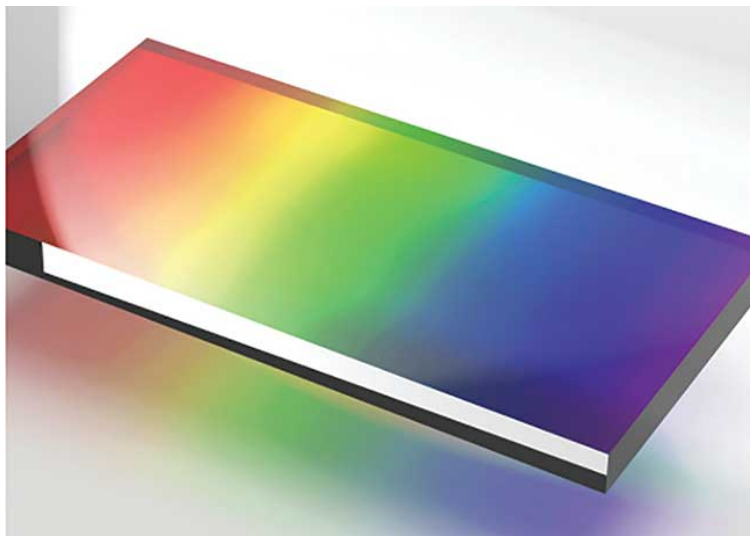


FIGURE 2.1: Linear variable optical filter.

To summarize, by physically moving the LVF across its X-axis we select a small

window of the LVF, effectively using it as a narrow band-pass filter. In order to acquire a full 400-1000nm spectral cube, we will move the LVF $\frac{1000-400}{step} + 1$ times and capture every image. The lens, sensor and scene / specimen must be perfectly still during the spectral cube acquisition. With a step of 5nm we will obtain 121 spectral images. In these "raw" images we have completely separated every component of different wavelengths, keeping only the target frequencies. Next, we will discuss the problems that arise in this design and our own method of reconstructing a proper spectral cube.

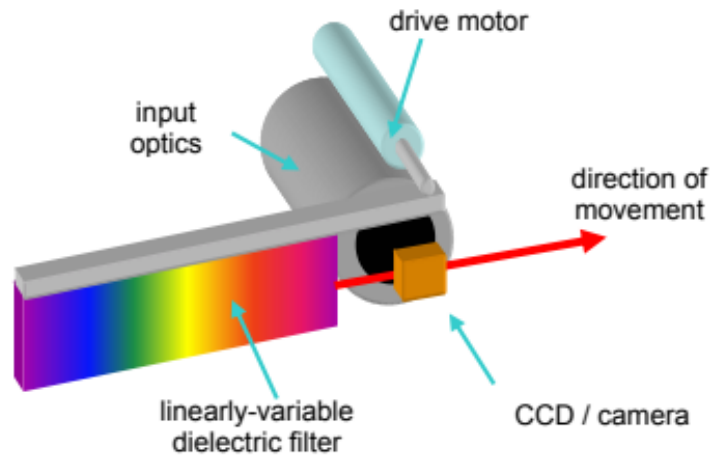


FIGURE 2.2: Linear variable optical filter with a motor.

2.2 The non-uniformity problem

We previously discussed how moving the linear filter helps us select a small window, simulating a band-pass filter. The main problem that arises due to the selection of this window is that our spectral image will retain the linear gradient throughout the picture.

This effect is most clearly visible using the following setup: we replace the mono (monochrome) sensor with a color (RGB) sensor and we move the linear filter to 590nm. The reason this band was selected was due to the properties of the Bayer filter installed on top of the RGB sensor. We can observe wavelengths deviations clearer near the fringes of each channel's response. As we can see in Fig. 1.3 the optimal bands are 485nm (where we observe differences between blue and green)

and 590nm (where we observe differences between green and red). Due to the high contrast between the colors red and green, I chose the band 590nm.



FIGURE 2.3: Acquired "raw" spectral image on 590nm.

As we can see in Fig. 2.3 this spectral image does not contain a single band (590nm), but a gradient of colors (frequencies) that we will later prove extends from 570 to 610nm. What we seek to accomplish is to **restore the monochromaticity** of all spectral images in a spectral cube. This process is extremely important, as our images lose spectral information that already resides within the spectral cube. For example, if we observe either the far left or the far right side of the image, we will retrieve data from 570 and 610nm, respectively, whilst the requested wavelength was 590nm.

2.3 Spectral deviation

The following experiment will programmatically calculate the standard deviation (σ_λ) of the light's wavelength in a spectral image. It is necessary to know the standard deviation of the spectral image's spectrum, as this knowledge will be vital to our reconstruction methods.

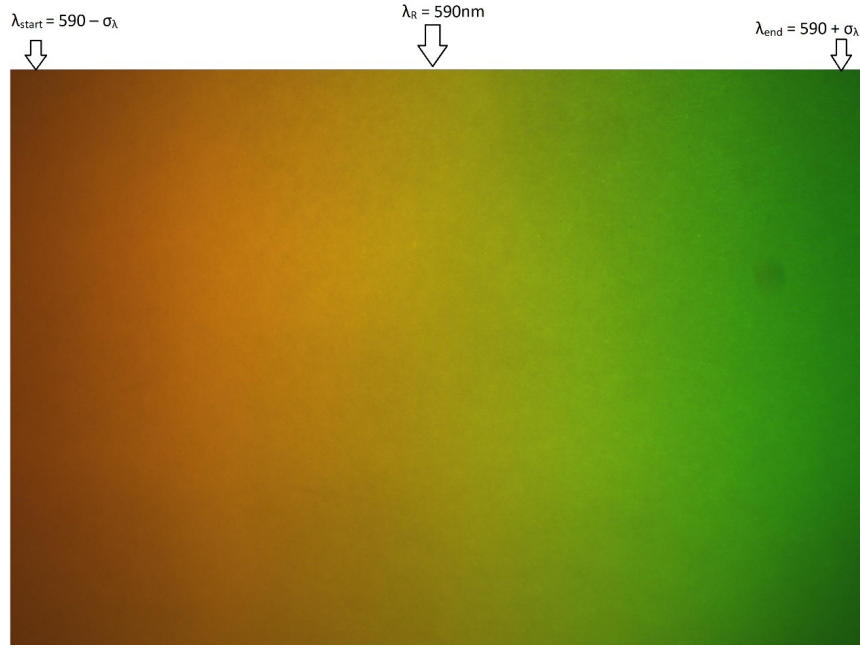


FIGURE 2.4: Standard deviation (σ_λ) of a spectral image's frequencies.

First, we captured a spectral cube of a fully reflective (white) target. This spectral cube contains all the spectral information we need for the linear filter. Our device has been calibrated so that all bands have normalized intensities. In Fig. 2.4 we can see some thumbnails of the spectral images (26 bands, 450-700nm, with a step of 10nm).

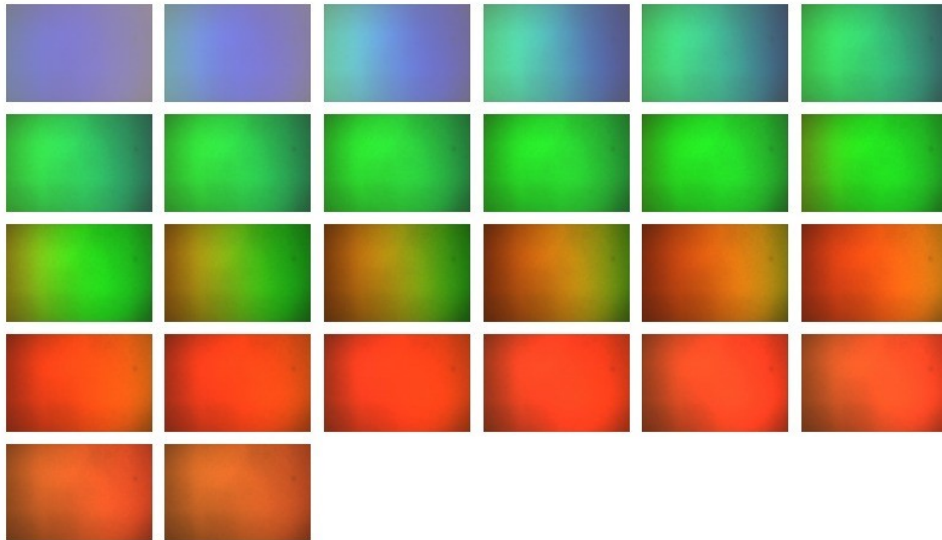


FIGURE 2.5: Spectral cube of a white target (450-700nm)

Second, we took samples from every image. We fragmented the center of every image in 30 pieces (per 100px). We consider that in this sampling rate every fragment

contains a unique RGB color.

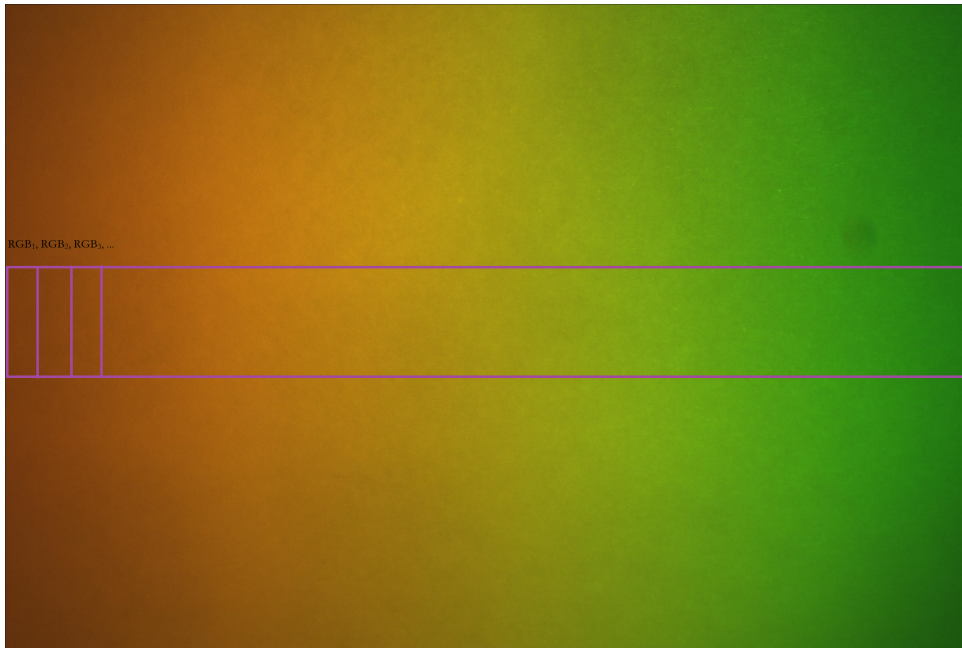


FIGURE 2.6: Sampling the spectral images.

Due to the linearity of the filter the same unique RGBs will be spotted in both preceding and following bands. The following figure contains all the cube fragments.

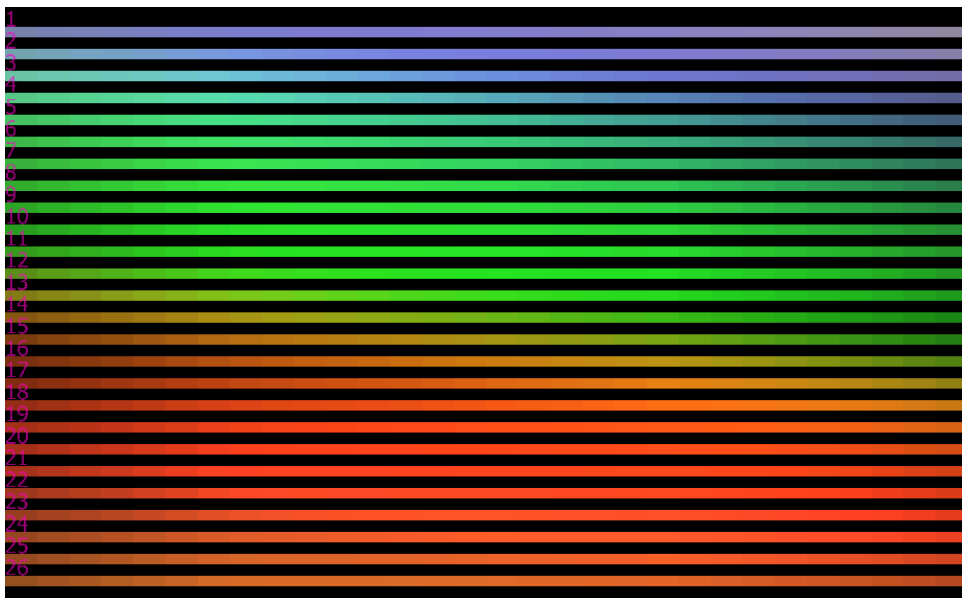


FIGURE 2.7: Cube fragments - Filter linearity

At this point, we have a 3-dimensional matrix that connects:

- Spectral information (wavelength of the pixel in the center)
- Spatial information (position of the fragment in relation to the image)

- Color information (a fragment's RGB color)

By combining this data into a heuristic algorithm, we located unique RGB in neighbouring bands. For example, in Fig. 2.8 we can see the positions of some unique RGBs.

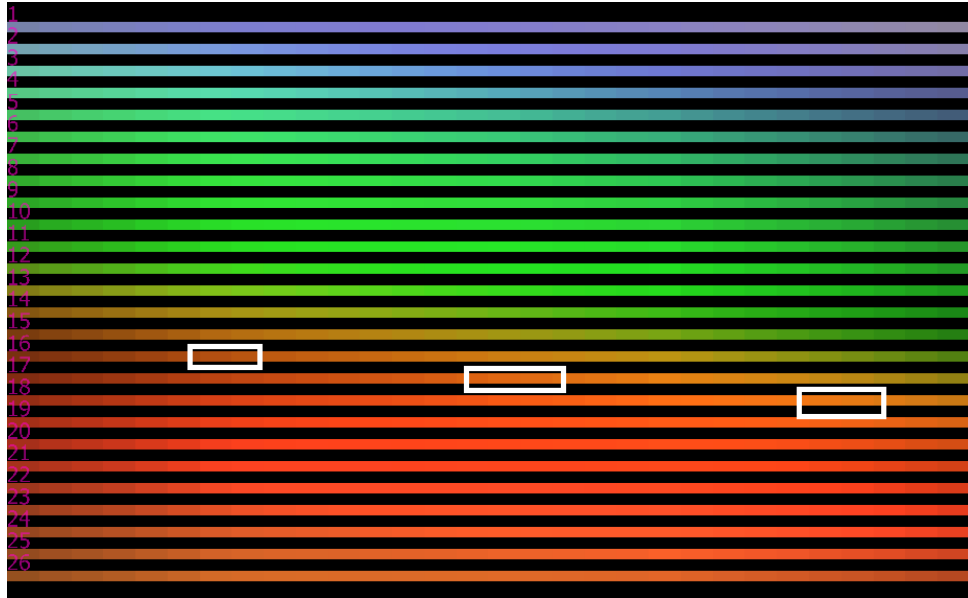


FIGURE 2.8: Filter linearity - Unique RGBs.

We know for fact that the center pixel has a wavelength of 610nm. Consequently, the left and right white rectangles both reflect the same wavelengths.

As it was previously explained, the bands we selected to calculate the final results were near 480 and 590nm, as these bands have the highest spectro-spatial fluctuations in the RGB color space.

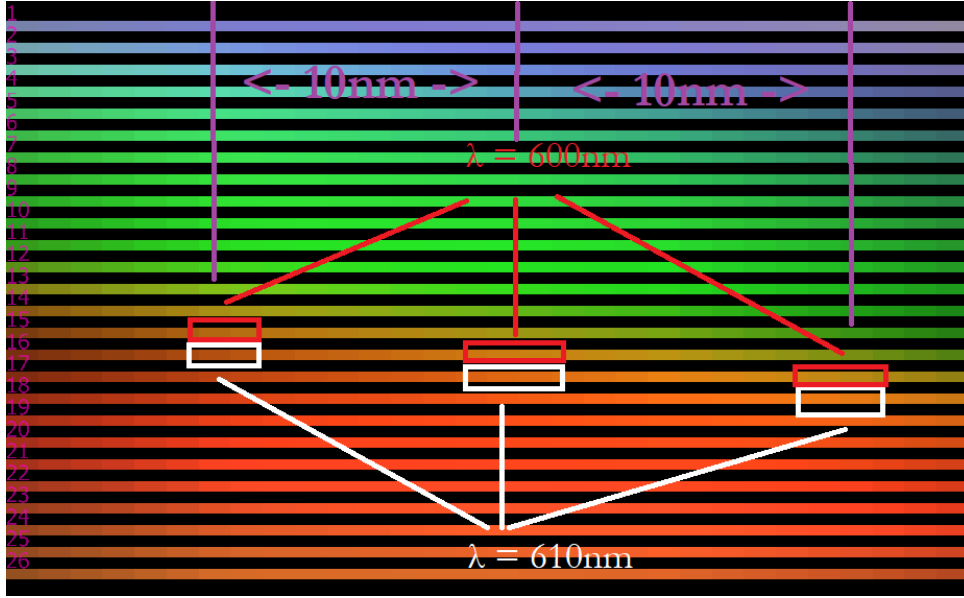


FIGURE 2.9: Calculating spectral deviations.

In the same manner, we found the left/right rectangle positions of the whole cube by comparing RGB colors with the center rectangle RGB color. Due to the high number of samples (law of numbers) the spectral deviation converged to $\sigma_\lambda = 19.86nm$.

2.4 Spectro-spatial mapping

Due to the linearity of the optical filter, we know for fact that the step of the gradient is fixed. Now that we know the wavelength of the first, middle and last pixel, we can create a map of pixel to wavelength correlation. With the knowledge of λ_R (requested wavelength, or else the wavelength of the middle pixel) and the filter's step we should be able to construct a map that links every column of 2.3 to a certain electromagnetic wavelength (see Fig. 2.10).

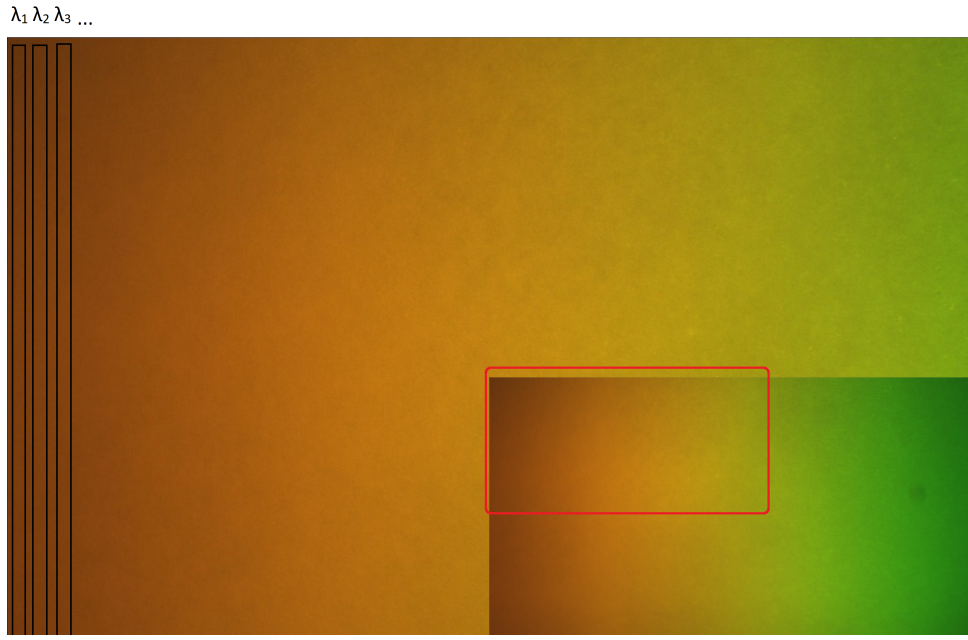


FIGURE 2.10: Map of pixel to wavelength correlation.

The requested wavelength λ_R is calculated using a digital spectrometer (Ocean Optics USB4000 VIS-NIR) with sub-nanometer accuracy. The only constant left to calculate is the step of the wavelength in subsequent pixels λ_{STEP} .

$$\lambda_{STEP} = \lambda_2 - \lambda_1 = \lambda_3 - \lambda_2 = \dots = \lambda_W - \lambda_{W-1}$$

where W = Image width in pixels.

Since we know both the middle wavelengths and the side wavelengths, then we can calculate λ_{step} as:

$$\lambda_{STEP} = \frac{\lambda_{middle} - \lambda_{left}}{\frac{W}{2} - pos_0}$$

where pos_0 = left unique RGB position in pixels,

OR

$$\lambda_{STEP} = \frac{\lambda_{right} - \lambda_{middle}}{pos_1 - \frac{W}{2}}$$

where pos_1 = right unique RGB position in pixels.

Given that we calculated both λ_R (using the spectrometer) and λ_{STEP} (with the above process) we may produce this spectro-spatial map for the full cube.

We can calculate a pixel's wavelength using the following formula:

$$\lambda_{pixel} = \lambda_R + \lambda_{step} * \left(\frac{W}{2} - pos_{pixel} \right)$$

λ_R is the wavelength of the middle pixel, or else the "requested" wavelength.

pos_{pixel} is the spatial location of the pixel along the X-axis of the image.

2.5 Tomographic cube reconstruction

In order to overcome the non-uniformity problem, we had to create a "tomographic" method to reconstruct the cube. This method is illustrated in Fig. 2.11.



FIGURE 2.11: Illustration of the tomographic reconstruction.

In this illustration, every horizontal set of blocks represents a **single spectral image**. Note that λ_{STEP} in this illustration is exaggerated. By combining fragments of every spectral image diagonally, with the assistance of the spectro-spatial map we created in the previous section, we may reproduce a fully monochromatic spectral

image. The quality of the reconstruction depends heavily on the step of the pixel to wavelength ratio (λ_{STEP}).

Our goal is to find relevant pixels (pixels whose wavelengths are close to the requested wavelength λ_R) from the neighboring spectral images and cut and paste them into the target image.

2.5.1 The downside of the tomographic method

Even though the tomographic method is a valid method for spectral reconstruction, the results are unsatisfactory. Our result images contain stripes due to the abrupt changes (discontinuities) of the spectrum. For example, if we cut and paste pixels from neighbouring spectral images, due to the gradient of the linear filter, the image spectrum would have a repetitive pattern: 408, 407.5, .., 400, 408, 407.5, The abrupt change between 400 and 408 will create an effect of discontinuity that seems instinctively faulty and/or mistaken. This effect which results to stripes is seen in Fig. 2.12.

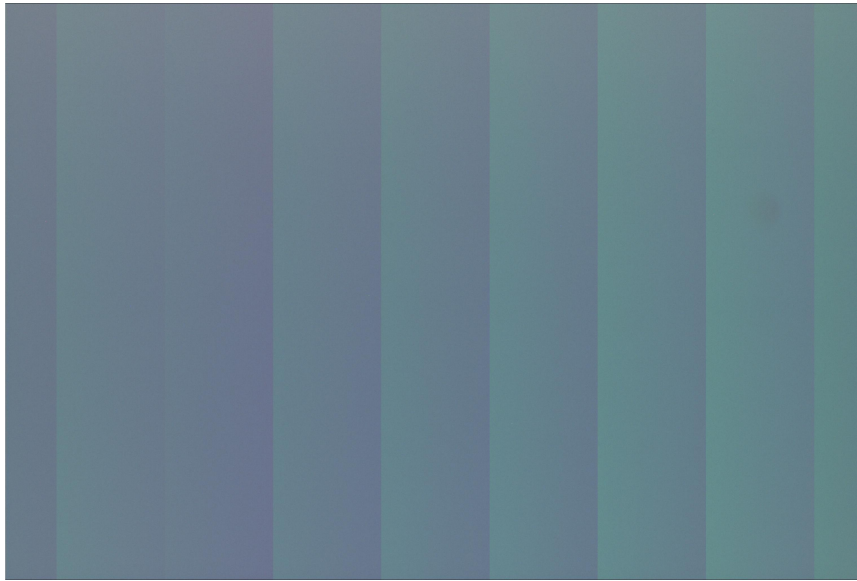


FIGURE 2.12: Tomographic reconstruction: stripe effect.

2.5.2 Enhancement by linear interpolation

In order to solve discontinuity issues, we applied linear interpolation to recover the missing gaps and eliminate these gradient filled stripes. To fully restore an image, we need to interpolate every pixel. For a 6MP image, this means we need to perform

6,000,000 interpolations.

The procedure goes as follows:

First, we select a pixel with coordinates (x, y) or (column, row) from a spectral image with wavelength λ_R . At this point we should remember that the pixel’s precise wavelength can be calculated using the formula in 2.4.

Second, we retrieve that pixel’s whole spectrum using the spectral cube. From the captured spectral cube, we shall retrieve every RGB or Gray value of that certain pixel from every image and construct its spectrum (RGB or Gray value versus wavelength), as seen in Fig. 2.13. This figure shows us how the whole spectrum is shifted towards the infrared due to the physical position of that certain pixel.

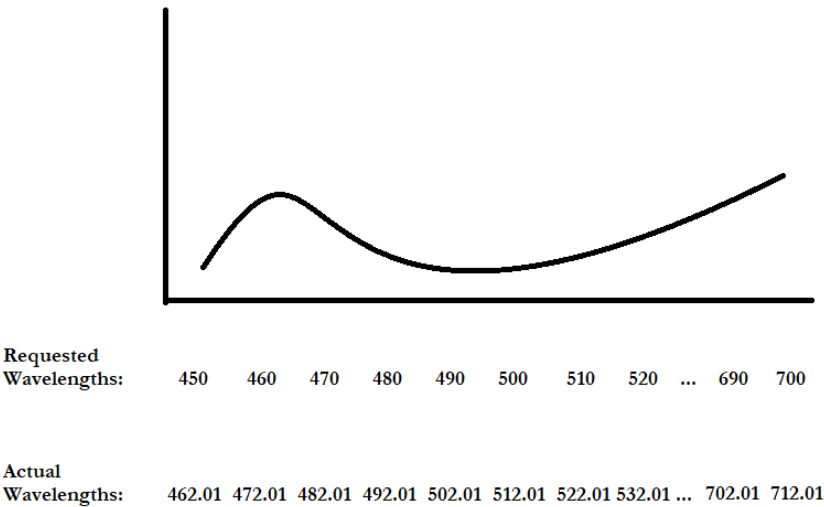


FIGURE 2.13: Spectrum: Requested and Actual wavelengths.

Third, we perform a linear interpolation of the value we require (see Fig. 2.14).
Algorithm:

- 1. Iterate until we get to Points A, B.
- 2. Calculate the slope and the position of Point C (with hardware acceleration).
- 3. Return the y-value of Point C.

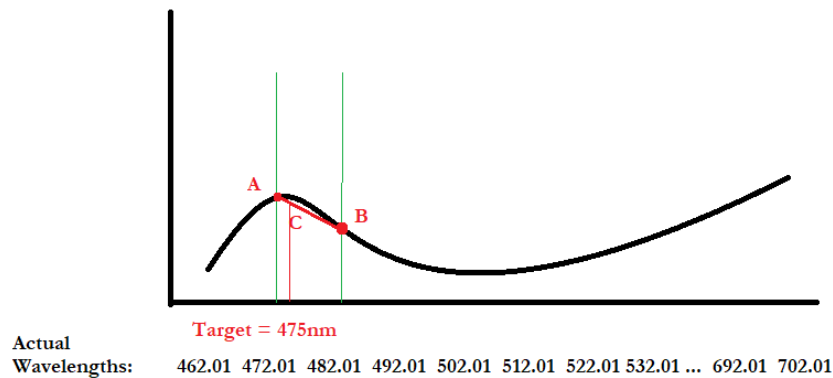


FIGURE 2.14: Linear interpolation on the shifted spectrum.

2.5.3 Improvements to the linear interpolation assisted tomography

The method of linear interpolation provides better results and removes any stripes and artifacts from our images due to discontinuities. There is however a lot of room for improvement.

Improvements in the spectral domain

Linear interpolation is the simplest, fastest method of interpolating (or guessing) values between two known points. Other algorithms may be used to provide more accurate results. For example, in Fig. 2.14 we can see that the estimated y-value of Point C is not on top of the curve. The error margins depend heavily on the sampling frequency and the nature of the scanned spectrum; if the object's spectrum has lots of sparks and changes to its gradient - which leads to curves - then linear interpolation might fail to estimate properly.

Linear interpolation is sometimes optimal due to its speed. Other spectral estimation algorithms may provide better, more accurate results. Whether we should use linear interpolation, spectral estimation algorithms, or none of the above depends heavily on the application, the accuracy we expect from the results and the amount of time we are willing to spend to improve our results. This is essentially a trade of accuracy for speed.

Following is a partial list of non-parametric spectral density estimation techniques:

- Periodogram, the modulus-squared of the discrete Fourier transform
- Bartlett's method is the average of the periodograms taken of multiple segments of the signal to reduce variance of the spectral density estimate
- Welch's method a windowed version of Bartlett's method that uses overlapping segments
- Multitaper is a periodogram-based method that uses multiple tapers, or windows, to form independent estimates of the spectral density to reduce variance of the spectral density estimate
- Least-squares spectral analysis, based on least squares fitting to known frequencies
- Non-uniform discrete Fourier transform is used when the signal samples are unevenly spaced in time
- Singular spectrum analysis is a nonparametric method that uses a singular value decomposition of the covariance matrix to estimate the spectral density
- Short-time Fourier transform
- Critical filter is a nonparametric method based on information field theory that can deal with noise, incomplete data, and instrumental response functions

Below is a partial list of parametric techniques:

- Autoregressive model (AR) estimation, which assumes that the n th sample is correlated with the previous p samples.
- Moving-average model (MA) estimation, which assumes that the n th sample is correlated with noise terms in the previous p samples.
- Autoregressive moving average (ARMA) estimation, which generalizes the AR and MA models.
- MULTiple Signal Classification (MUSIC) is a popular superresolution method.
- Maximum entropy spectral estimation is an all-poles method useful for SDE when singular spectral features, such as sharp peaks, are expected.

Improvements in the temporal domain

Improvements may also be made in the temporal domain, to boost the speed of these procedures. Linear interpolation may be parallelized in the CPU with multiple worker threads, or even better in the GPU. The approach we chose to follow is hardware acceleration using the GPU, using OpenCL.¹

The process of reconstructing RGB cubes using our method of tomography with linear interpolation required 21-26 secs per spectral image in a serial implementation. A spectral cube captured by our device may contain up to 121 bands. Our hardware accelerated optimizations led to a staggering 1.7-3 seconds per image (this figure is GPU dependent), leading up to **12.3x shorter** processing times.

2.5.4 Validation of tomographic method with interpolation

Gray values vs RGB

The procedure above has revealed the true correlation of pixel position vs wavelength. Thus, upon the replacement of the RGB sensor with a monochromatic sensor, there will be no need to develop a new procedure. This procedure is in fact an exploitation of the 3D RGB color space, with whom we are able to calibrate any device (the final product can be either RGB or Monochromatic). The only requirement for monochromatic devices is to temporarily install an RGB sensor just for the calibration and then remove and replace with a monochromatic one.

The reason why we would rather install a monochromatic sensor is because we want to avoid the BGR filter cutoffs. A hyperspectral imager is a scientific instrument, destined to deliver images with a minimal error. Should an RGB sensor be used, the image would be subjective due to the three visible filters cutting off certain frequencies and overlapping one another.

¹OpenCL is a C++ library that allows the use of a Graphics Processing Unit to speed up either basic or complex calculations.

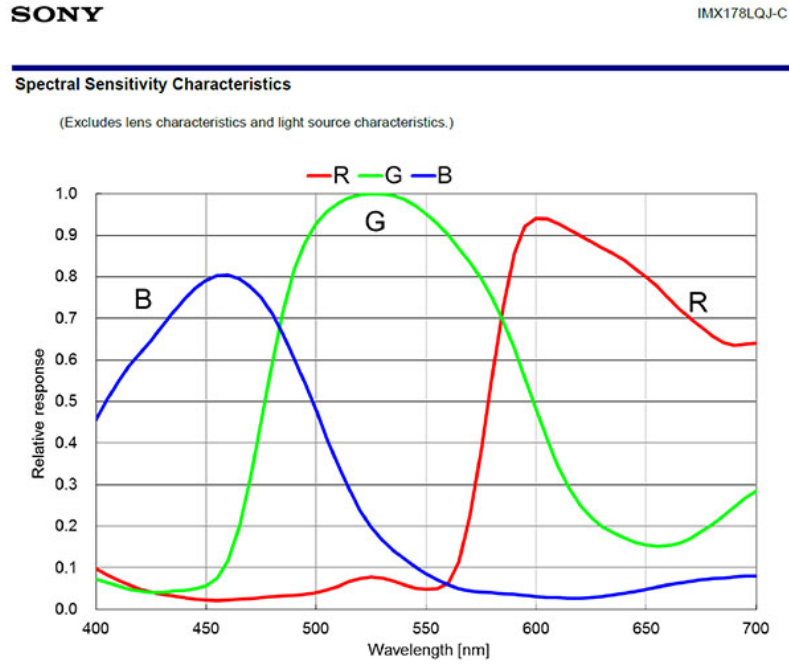


FIGURE 2.15: RGB camera spectral response (Sony IMX178).

Minimum requirements

The procedure's results have shown that in our device, the standard deviation of the light's wavelength is $\pm 19.86nm$. So, in order to produce an accurate map of pixel column vs wavelength, we would need a cube with a step of at most 19.86. For this experiment we chose 10nm, so we can be closer to the center, where the lighting conditions are more homogenized. Generally, the cube's maximum step is proportional to the distance of the sensor against the linear filter. To construct a map of the highest accuracy, we would require:

- fully homogenized lighting throughout our target
- pure white light source(s)
- a non-absorbent white target
- a spectral cube with the maximum possible step

To explain the latter, by using the maximum step, the left and right barriers (purple bars in Fig. 2.9) would stretch to their maximum, providing higher accuracy. Next, we will discuss the smallest achievable margin of error.

Margin of error

Spectral imaging is superior to spectroscopy, in the sense that we acquire spatial information in contrast to plain single values. There is a slight disadvantage that needs to be considered though, and that involves the cross-talking between neighboring pixels, mainly caused by the MOSFETs' parasitic inductance and capacitance. For these reasons, we conducted an experiment to observe the differences between neighboring pixels. We used the sensor SONY IMX178. For this specific sensor, the cross talking and noise phenomena will interfere with our pixel intensity values at about $\pm 3-4$. The RGB value drops by 3.43 on average every 100px. We conclude that our average error is equal to:

$$\epsilon_{avg} = \lambda_{step} * 100 = 0.013 * 100 = 1.3nm$$

Results of reconstruction

Below we can see the results of our spectral cube reconstruction method. Figure 2.16 shows the thumbnails of a spectral cube acquired by our device. We chose an RGB cube because the gradient effect is more visible.

Figure 2.17 shows the thumbnails of the spectral cube after the reconstruction. We can observe that the gradient effect has completely disappeared. The average error, as calculated in the previous step, is 1.3nm.

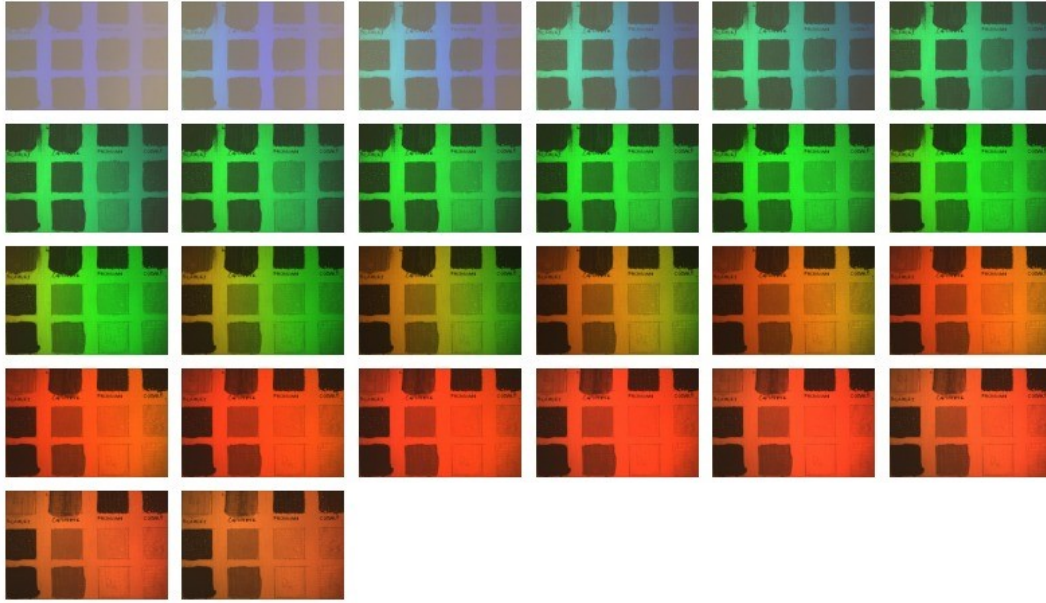


FIGURE 2.16: Acquired RGB spectral cube.

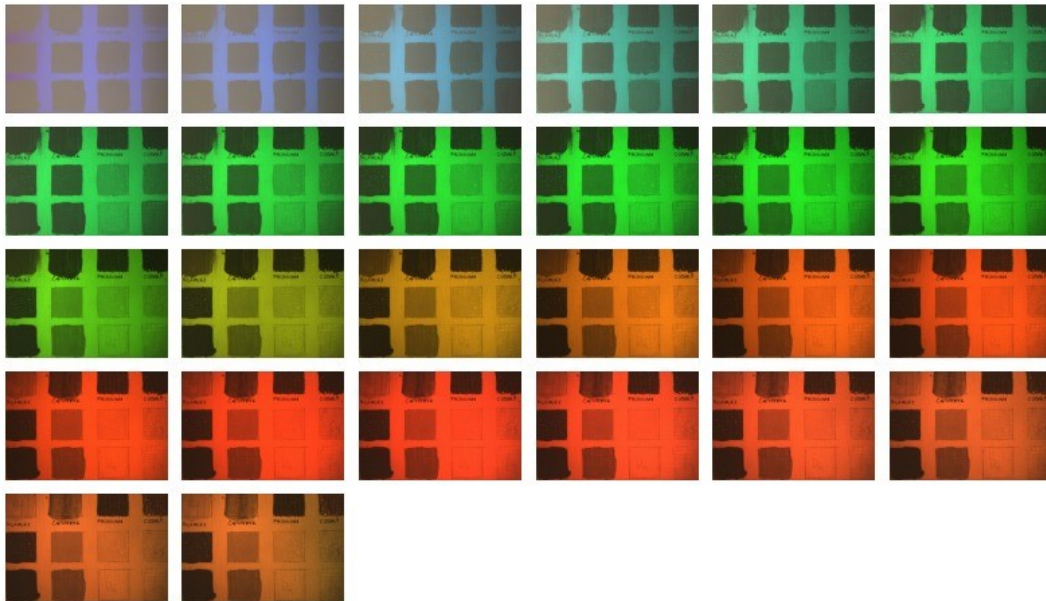


FIGURE 2.17: Reconstructed RGB spectral cube.

The figure below (2.18) will showcase the hardest band to reconstruct: 590nm. 590nm is the point where the green and red filters' spectra converge. Any mistakes during the calculation of the spectrospatial maps are visible to the naked eye due to the high chromatic contrast between the red and green colors. As we can see, the result is a perfect amber color, which represents the 590nm.

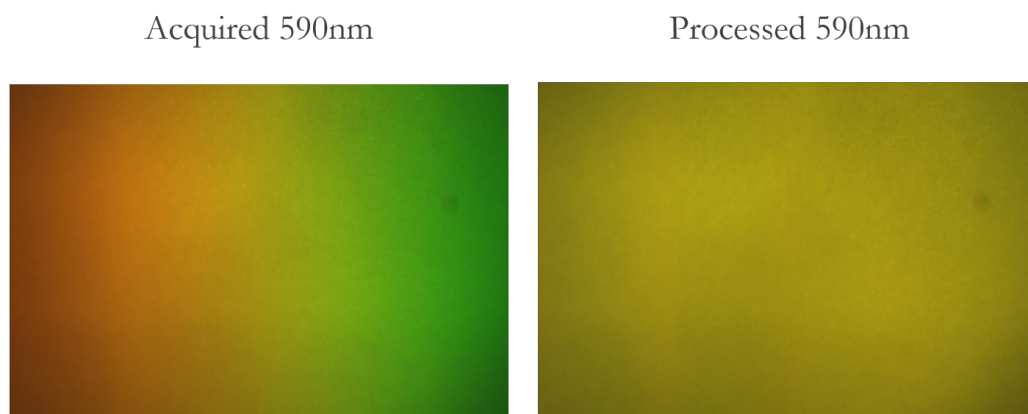


FIGURE 2.18: 590nm reconstructed.

Chapter 3

Hardware

3.1 Muses9-HS

Muses9-HS is a spectral-scanning staring type hyperspectral imager. As we mentioned in Section 1.5.3 spectral scanning HSIs feature some unique advantages, such as very high spatial resolution, high spectral fidelity, and others.

This device consists of the following interchangeable components:

- Lens 16 or 25mm (depends on the desired scene width)
- Linear variable optical filter
- RGB or Monochrome CMOS sensor (Sony IMX178)



FIGURE 3.1: Muses9-HS1700

The following table contains its specifications:

Wavelength tuning range	370-1700nm
Bandwidth (FWHM)	5-20nm (370-1000nm)
Light throughput (efficiency)	75-95% (unpolarised)
Tuning speed	Few seconds or even snap-shot/real time
Control	Computer control
Operation modes	Color and Spectral Imaging
Sensor-type	CMOS and InGaAs
Sensor dimensions	1/1.8" (CMOS), 1" (InGaAs)
Thread	C-mount or F-mount
Resolution	6.4 Mega Pixels (C-MOS), VGA (InGaAs)
Interface / Data Acquisition Protocol	USB3.0
Working Temperature	-5C to 45C
Data transfer speed	Higher than 1Gbps (USB 3 or GbEth)
Sensor's cooling	Not necessary due to high light throughput
Lens	C-Mount or F-mount lens.

3.1.1 Muses9-HS: Linear variable optical filter

The device contains two filters, one of which was cut so we can achieve a full spectrum continuum, in the range of 400-1000nm.

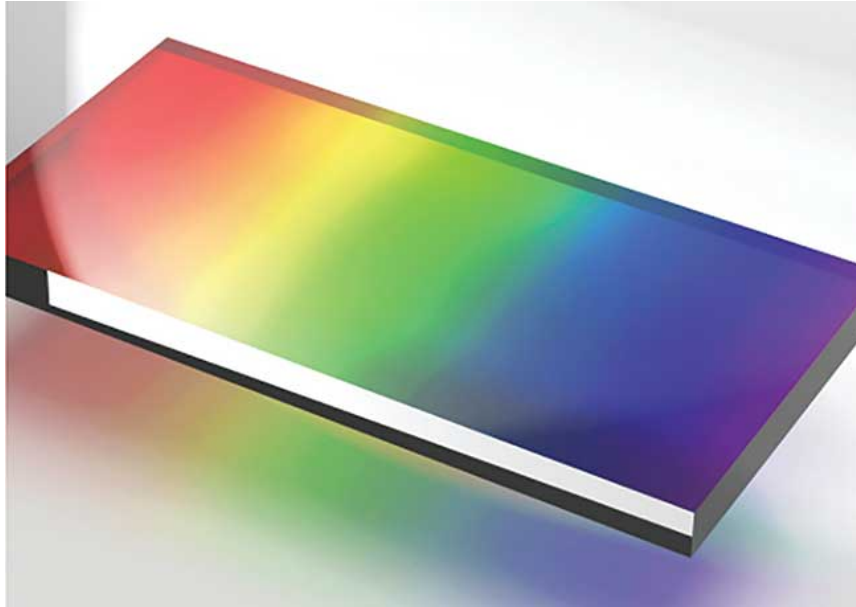


FIGURE 3.2: Linear Variable Filter.

The first filter is the Linear Variable VIS Bandpass Filter by Edmund Optics. This filter will cover the area around 400-700nm.



FIGURE 3.3: Linear Variable Filter response.

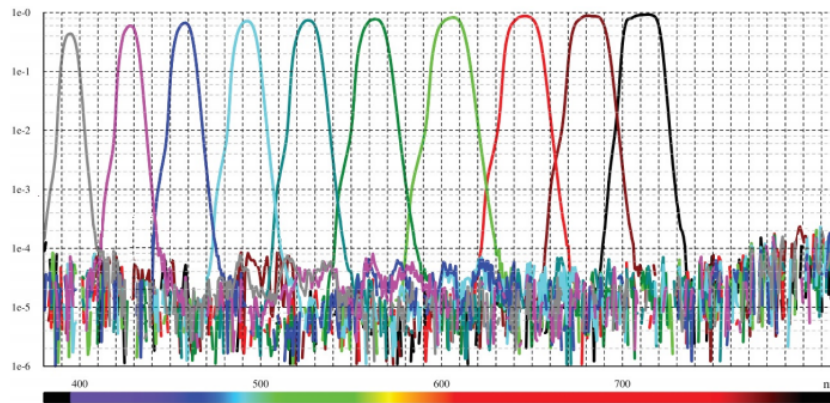


FIGURE 3.4: Linear Variable Filter blocking ability.

The following table contains its specifications:

Optical Density OD	≥ 4.0
Transmission (%):	> 95
Bandwidth (nm):	50%: 7-20 0.1%: 13-34
Optical Density Steps:	Average: >4.0 Minimum: >3.0
Thickness (mm):	2.50
Type:	Bandpass Filter
Coating:	Variable
Dimensions (mm):	60.0 x 12.0
Aperture (mm):	0.5 x 10.0
Substrate:	Fused Silica
Transmission Steps (%):	40 to 95 (Average)
Wavelength Range (nm):	400 - 700

The second filter is the Linear Variable NIR Bandpass Filter by Edmund Optics. This filter was cut by a specialist (an optician) from 550-699nm, and we only used the part that allows wavelengths 700-1000nm.

The following table contains its specifications:

Optical Density OD	≥ 4.0
Transmission (%):	> 90
Bandwidth (nm):	50%: 7-20 0.1%: 20-60
Optical Density Steps:	Average: >4.0 Minimum: >3.0
Thickness (mm):	2.50
Type:	Bandpass Filter
Coating:	Variable
Dimensions (mm):	60.0 x 12.0
Aperture (mm):	0.5 x 10.0
Substrate:	Fused Silica
Transmission Steps (%):	40 to 95 (Average)
Wavelength Range (nm):	550 - 1000

3.1.2 Muses9-HS: CMOS Sensor

The sensor we have chosen is Sony IMX178. The rolling shutter CMOS sensor Sony IMX178 provides very high resolution of 6.41 MP (3088 x 2076 px), which makes it especially perfect for visualization tasks in microscopy, medical engineering, and quality assurance. Due to its high speed, it is also considered as a cost-driven option for traffic monitoring (ITS). The BSI sensor of Sony's STARVIS series is one of the most light-sensitive sensors in our portfolio, and therefore, it offers an amazing image quality even in low-light conditions. Due to its 1/1.8" sensor size, a wide range of wide-angle lenses is available. In combination with our USB 3.0 industrial cameras, the Sony IMX178 delivers frame rates up to 58 fps at full resolution. *Sony IMX178*

This CMOS sensor is controlled by a chip provided by QHYCCD. QHYCCD is one of the leading companies in AstroImaging equipment. The models we used are QHY5-III-178M (Monochrome) and QHY5-III-178C (RGB Color).



FIGURE 3.5: QHY5-III-178

Sensor	Sony IMX178 Exmor CMOS sensor (Mono/Color)
Imager Size	Typical 1/1.8-inch
Effective Pixels	3072 x 2048 6 Megapixels
Effective Area	7.37mm x 4.91mm
Pixel Size	2.4um x 2.4um
Readout Type	Progressive Scan
Full Well	15ke-
Readout Noise	2.4e - 0.9e
Anti-amplight Control	Yes (Reduces amp glow significantly)
Shutter	Electronic Shutter
Max Frame Rate	50FPS @full resolution 100FPS@1528x1024 190FPS@764x512
ADC Sample Depth	10/14-bit, Output 8-bit/14-bit
Exposure Time	9us - 1200sec
Pixel Binning	1x1, 2x2
MicroLens	Yes, on-chip microlens array
Peak QE	TBD
Guide Port	Yes, 5-pin Lemo aviation socket
Back Focal	Approx. 11mm
Camera Size	1.25-inch Eyepiece Size (D=31.6mm)
Optic Window	AR+AR(Mono) AR+IR cut 680nm (Color)

The figure below shows the Readout noise vs the Analog Gain.

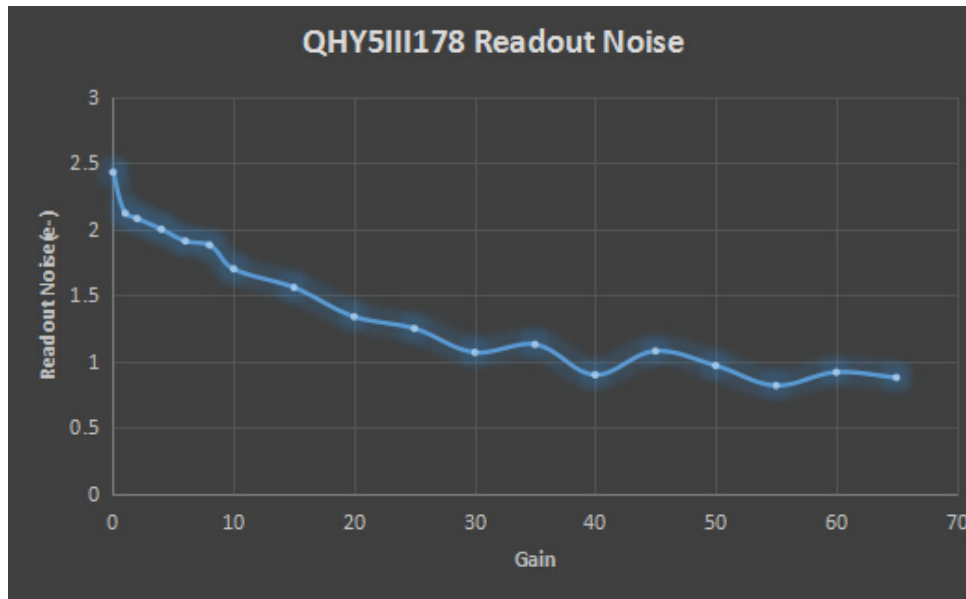


FIGURE 3.6: QHY5-III-178 readout noise.

3.1.3 Motorized system

This system can obtain spectral cubes with a single button. This means that there is no need for manual tuning, the user may select the desired wavelength using the software and the LVF will move to the exact position that will display that specific wavelength. This feature is implemented using an Arduino Nano.

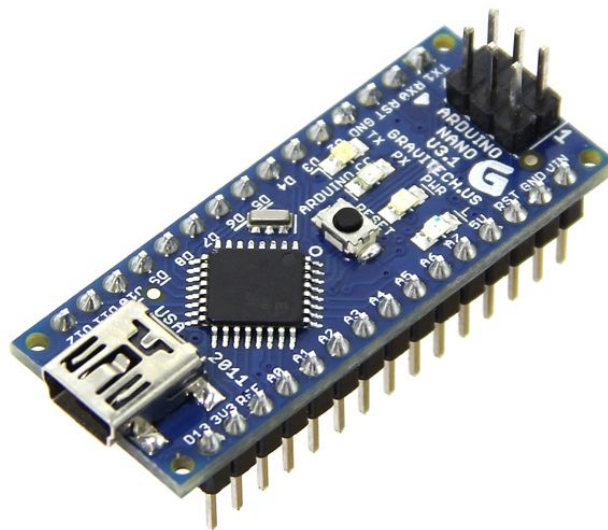


FIGURE 3.7: The Arduino Nano.

Chapter 4

Software

4.1 Muses9 Spectral Suite

For the purposes of this thesis, a GUI software had to be developed. This software is the result of work completed by previous coworkers, and improved/customized for use in this project.

4.1.1 Modes of operation

This device can operate in two modes: Spectral Imaging and Spectral Cube Acquisition.

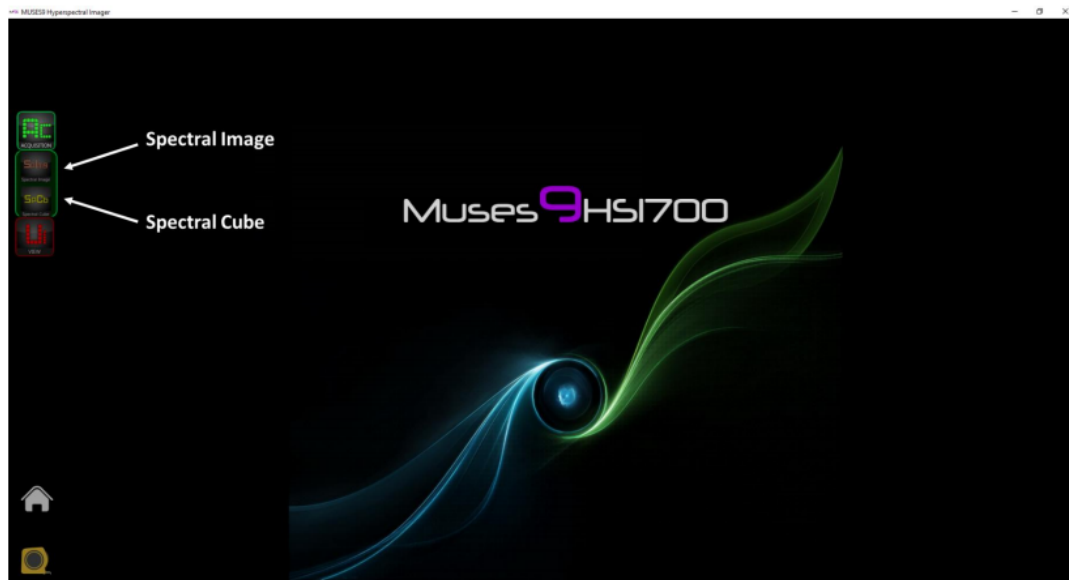


FIGURE 4.1: Software: Modes of operation

Spectral Imaging

In this mode we can observe any spectral band live. Of course, the tomographic scanning method does not apply here, as in this mode the device operated as a no-scanning, realtime, snapshot spectral imager. The user may tweak the sensor's exposure time and analog gain. The GUI allows us to select a wavelength in the right side of the window. The rainbow-colored bar represents the visible spectrum that is viewed using the CMOS sensor and the 1100, 1200, .., 1600 buttons above this bar allow us to view discrete ShortWave-IR bands using an InGaAs sensor. The SWIR bands have no use in Quantitative Pathology so far, so we will focus primarily on the visible spectrum. The "Photometry" label allows us to view the average intensity of a block of pixels. The user may select the Region of Interest by clicking on the image and the photometry label will update every few frames. Other useful features include freezing, saving and zooming the video feed.

This mode does have a use in Quantitative Pathology, as the examiner may use pigments and select their peak wavelength from the GUI. The pigments will appear bright white (high reflectance, low absorbance), while the rest of the element will range from black to light gray. This mode is especially useful because it is live (no delays, real time video feed), allowing the examiner to view the whole sample with great haste.

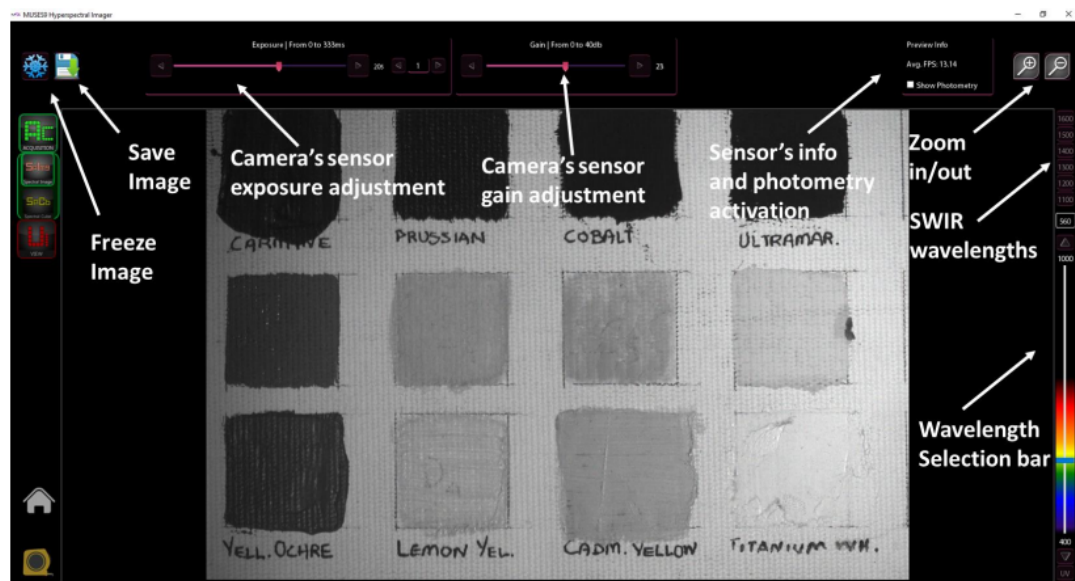


FIGURE 4.2: Software: Spectral imaging

Spectral Cube Acquisition

In this mode we may view the live feed (Visible-Near IR only) and tamper with the sensor's parameters, but the main focus is the automated cube acquisition process. The user may select a range of bands, spatial and spectral resolution of the images from the GUI. When the automated process begins, a thread will start changing the bands from the left border (first band) of the requested spectral range up to the final band.

While changing the bands, the software will load a pair of values from a generated calibration file (see Section 4.1.3 for more detailed information about the calibration of the device). This calibration file is a map that links a wavelength with a pair of Gain and Exposure values. The thread will load this values onto the sensor, move the motor to the appropriate wavelength and save the spectral image. After saving all the spectral images (with a 5nm fixed step) the post-processing algorithms will improve the quality and spectral fidelity of the cube. First, the images are divided by their reference values in order to reduce the stripe effect. Then, the tomographic process will interpolate the correct value of every single pixel in the spectral cube. The result can be viewed either within the folder that contains the cube or with the viewer we built inside the suite (see 4.1.2).

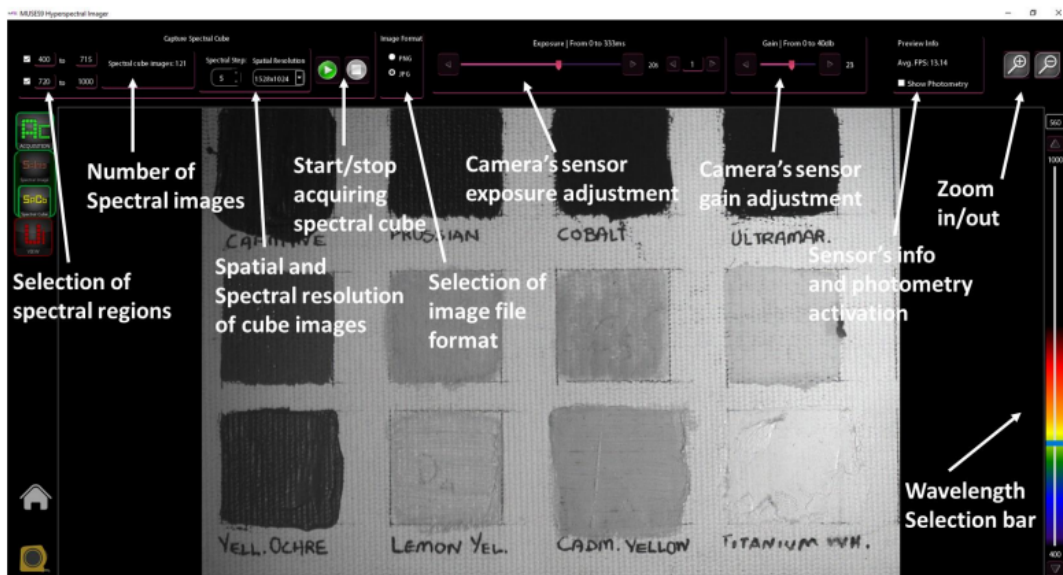


FIGURE 4.3: Software: Spectral cube acquisition

4.1.2 Spectral cube analysis

The spectral software suite allows the user to load and view any spectral cube that was previously captured and saved by the same software suite (see Fig. 4.4). The bar on top allows us to view a certain spectral band within the spectral cube. Within this suite we incorporated some tools that are extremely useful in Quantitative Pathology. First of all, the examiner may hover the mouse on any pixel and view its full spectrum on a floating window. The pixel's spectrum may be pinned by clicking on it. This way, we may display multiple spectra on top of each other. This feature may prove useful when we need to compare the spectra of two distinct positions. These two separate positions may point to different pigments, for instance, allowing the user to examine thoroughly the spectrum of every substance in every position.

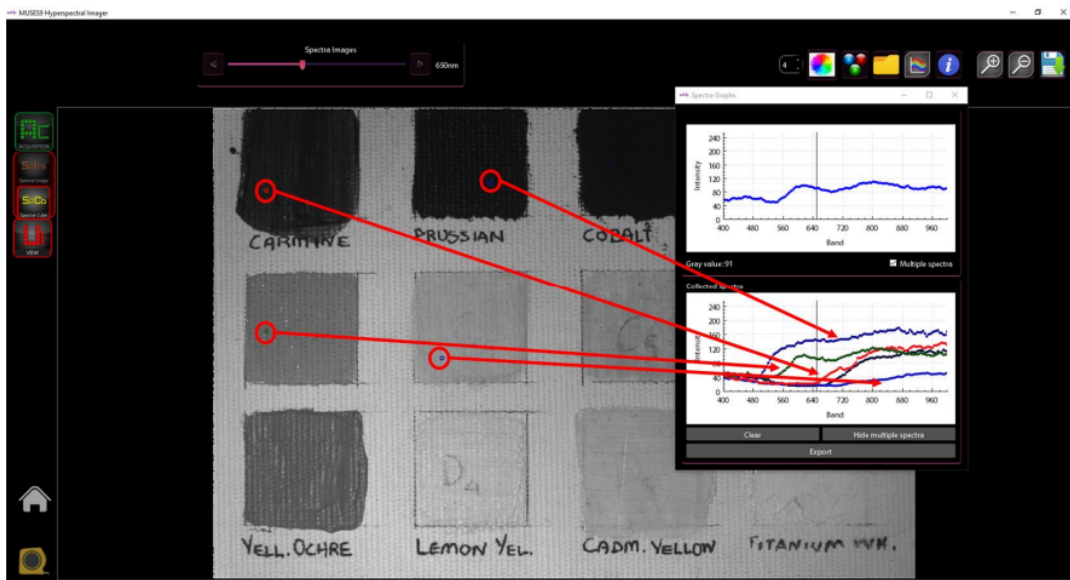


FIGURE 4.4: Software: Viewing spectral cubes

The software also has two more interesting features, the RGB color reconstruction (reconstruct a vivid colored image from the spectrum) and a clustering algorithm. For the clustering we implemented from scratch a widely used algorithm, k-Means. Our k-Means implementation will receive as input the whole spectral cube along with the preferred number of classes and will output a pseudocolored map (see Fig. 4.5). In this example, we ask for 4 classes, and the algorithm will place every pixel to its nearest class. As we can see, k-Means associated all the blue pigments together (green color), all the brown pigments (white color), the yellow pigments (red color)

and the white pigments (blue color) with great success. This feature is especially useful in Quantitative Pathology, as this automated process can find all the stains (e.g. hematoxylin and eosin) and associate them with the appropriate group. Such a map can make the work of a pathologist a lot easier, as it automatically spots all the regions of interest, no matter how small.

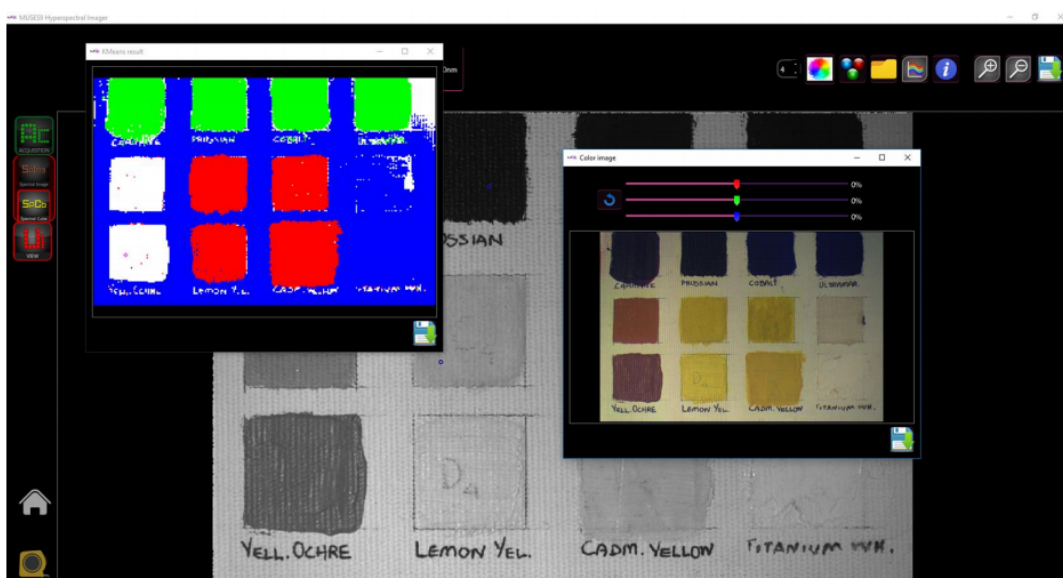


FIGURE 4.5: Software: Clustering with k-Means

4.1.3 Calibrating the device

This process is essential to the technical validation of this device. Every CMOS sensor has a certain quantum efficiency (see Fig. 4.6). Quantum efficiency is essentially the sensor's output (intensity) versus wavelength. As we can observe in the figure below, some wavelengths (mostly the green ones) have higher output than the rest. Others may be less sensitive. The same effect happens to the linear variable optical filters (see Fig. 4.7). So how can one calculate all these parameters, along with the lens and beam-splitter absorbances?

The answer is we don't have to. In order to solve this problem, we have devised a method that brings the device's output to a perfect equilibrium with the light-source.

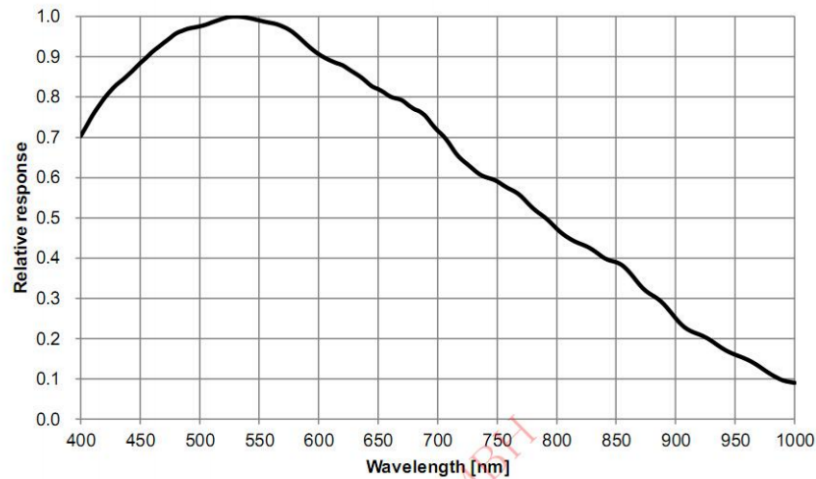


FIGURE 4.6: Sony IMX178M (Monochrome) Quantum Efficiency (QE)

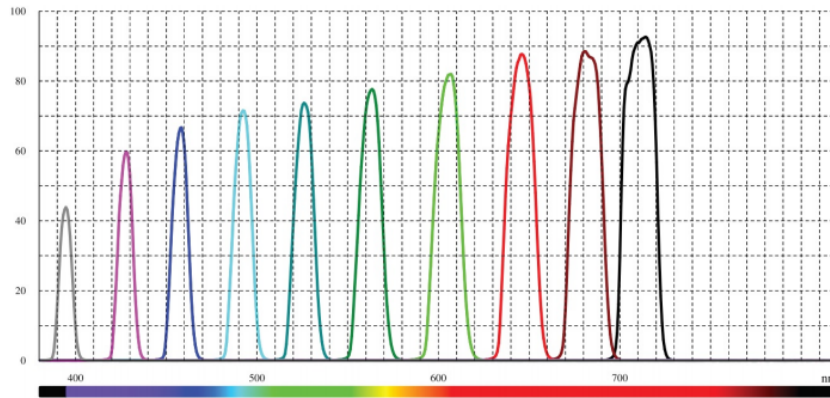


FIGURE 4.7: Linear Variable Filter response.

The process has a simple objective; the device must output (at the middle pixel) a constant intensity (the intensity is a plain number from 0-255) for every single band. When the process starts, we may set a standard intensity (e.g. 180). For every available wavelength, a thread will start tweaking the sensor exposure time and analog gain. When the intensity reaches the standard we set earlier within an acceptable error, we save the pair of gain and exposure to a calibration file. This calibration file is actually a map that links pairs of exposure and gain to a certain wavelength. Whenever the motor moves the filter to a new position, the sensor will update its parameters (exposure, gain) to match that specific wavelength. This is how our device stays completely calibrated and fully adaptable to any light-source, LED, halogen, UV, even the sun.

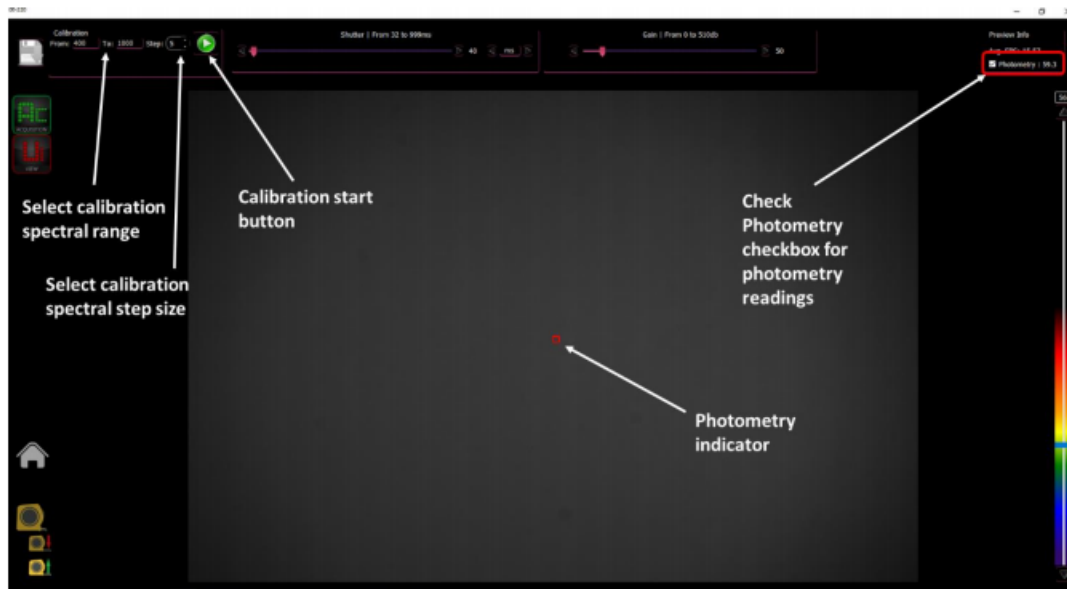


FIGURE 4.8: Software: Calibrating the device

Chapter 5

Quantitative Pathology

Quantitative analysis of histo- and cytochemical components such as DNA, RNA or chromatin pattern on one hand (cytometry) and the quantitative analysis of geometric non-chemical cell and tissue components (morphometry and sterology) on the other, have developed somewhat independently. Today, many different techniques, such as morphometry, sterology, and static image and flow cytometry are well established and routinely used in diagnostic quantitative pathology. The potential significance of these techniques in the individualization of care in cancer patients include the objective distinction between benign, borderline and malignant lesions, objective grading of invasive tumours, prediction of prognosis, and therapy response. [Buhmeida, 2006]

5.1 Morphometry

Morphometry is used to denote the interactive quantitative analysis of single cells or tissue sections by means of an eyepiece graticule, a projection microscope or a graphic tablet. It is a simple, inexpensive, relatively fast technique, and allows the quantitation of both cell and architectural (tissue) properties. Standard cell and tissue preparations can be employed for such investigations. This requires (minimal) standardization of the cell and tissue handling process. The degree of acidity (pH) of the fixation fluid, such as "neutral" (or buffered) formalin is probably the most important and easy to measure factor, and should be kept between 6 and 8 in order to obtain reproducible nuclear area measurements. Another important factor for reproducible results is the magnification in relation to the size of the particles measured.

Careful selection of relevant areas, cells and nuclei done by a skilled pathologist, is often essential, as well as quality control of the measuring process. [Baak, 1987]

When sampling, we are dealing with two types of morphometry. Group morphometry and diagnostic morphometry must be understood as two different approaches in histopathology. [Collan et al., 1987]

5.1.1 Group Morphometry

In group morphometry (statistical morphometry) we are dealing with samples taken from several patients or animals and these samples are studied with morphometric methods. Such studies can be principally of two types: prospective or retrospective. The latter two differ in terms of variation sources. In the prospective studies patient selection can be done with care, and the samples can be taken and processed in a uniform fashion. In the retrospective study samples are collected from the files of a pathology laboratory and the investigator cannot influence the primary selection of patients or the processing. However, in respect to cutting, staining and morphometric measurements these studies are equal. [Collan et al., 1987]

5.1.2 Diagnostic Morphometry

In theory, diagnostic morphometry can be as well controlled as group morphometry in prospective or retrospective studies. Usually, however, we are dealing with a situation which could be described as a third kind of study, the diagnostic study. This is an ongoing study which is being performed in different diagnostic laboratories and in which numerous investigators are participating. Most of them in fact do not know that they are investigators in a diagnostic study which is here characterized as a statistical investigation. In a diagnostic study the variation sources are much more numerous than in traditional prospective or retrospective studies. The studied population consists of samples of individual patients studied one at a time. The results of this investigation have an immediate relevance to the patient, because decisions about the treatment are dependent on the outcome of the investigation. In retrospective and prospective studies the outcome of the investigation need not necessarily have any specific influence on the treatment of the studied individual patients, but

may influence the treatment of other patients after the study has been completed. It has to be considered that in diagnostic studies morphometric measurements are not necessarily made in an identical fashion, and this is due to the fact that different laboratories and investigators use different methods. [Collan et al., 1987]

5.2 Cytometry

Cytometry is the measurement of the characteristics of cells. Variables that can be measured by cytometric methods include cell size, cell count, cell morphology (shape and structure), cell cycle phase, DNA content, and the existence or absence of specific proteins on the cell surface or in the cytoplasm. [*International Society for Advancement of Cytometry*] Cytometry is used to characterize and count blood cells in common blood tests such as the complete blood count. In a similar fashion, cytometry is also used in cell biology research and in medical diagnostics to characterize cells in a wide range of applications associated with diseases such as cancer and AIDS.

5.2.1 Static cytometry

In static cytometry, a relatively popular application is the measurement of the DNA content of single cells in slides. Although having the advantage of optical control, the measuring technique of the transmission systems is, at the present state of development, laborious. This restricts the measurable number of cells to one hundred or only a few hundred at maximum. As a result, the reproducibility rate, as well as the capacity to detect small differences is only moderate. It is expected that in the near future, very fast static DNA cytometers will become available, which measure the DNA content with a low coefficient of variation (nearly as low as currently possible with flow cytometers). [Baak, 1987]

5.2.2 Flow cytometry

With flow cytometry, in contrast to static cytometry, thousands of cells can be measured in suspension within a few minutes. This can not be used only with freshly

prepared tissue, but also with paraffin-embedded retrieved archival material. However, flow cytometry does not allow for the analysis of architecture-related features. There is also no direct visual control during the measuring process and the instruments used are rather expensive. Digital Image Processing (DIP) computers, in general, are somewhat less expensive than flow cytometers. They have the capacity to measure large numbers of objects at a reasonable speed, as well as architectural features of tissue. It is expected that with the further development of dedicated software, DIP computers will be able to cover most of the quantitative analyses in a pathology laboratory, most likely occurring (in a highly automatized) interactive way. [Baak, 1987]

In 1953 Crosland-Taylor published an unsuccessful attempt to count red blood cells using microscopy in which he solved the problem of aligning cells by using sheath fluid to hydrodynamically focus the cells. [Steinkamp, 1973] In the late 1960s, Van Dilla at Los Alamos National Laboratory built the first non microscopy-based cytophotometer. He did this by combining Crosland-Taylor's breakthrough with the fluorescent dyes originally developed for microscopy and a laser-based fluorescent detection system — the flow cytometer as we know it today. [Sack, Tárnok, and Rothe, 2009] Fulwyler, at Los Alamos as well, combines the Coulter principle with continuous inkjet printer technology to create the first cell sorter in 1965. [Fulwyler, 1965]

In 1973 Steinkamp and the team at Los Alamos follow up with a fluorescence-based cell sorter. [Steinkamp, 1973]

In 1978, at the Conference of the American Engineering Foundation in Pensacola, Florida, the name pulse cytophotometry was changed to flow cytometry, a term which quickly became popular. [GmbH, 2013] At that point pulse cytophotometry had evolved into the modern form of flow cytometry, pioneered by Van Dilla ten years earlier.

5.2.3 Cytophotometry

By the early 1930s various firms manufactured ultraviolet fluorescent microscopes. The stage was set for cytometry to now go beyond the now established hemocytometer. At this time, Torbjörn Caspersson, working at the Karolinska Institute in Stockholm, developed a series of progressively more sophisticated instruments called cytophotometers. These instruments combined a fluorescent microscope with a spectrophotometer to quantify cellular nucleic acids and their relation to cell growth and function. Caspersson's early apparatus now seems hopelessly primitive. But, even this primitive apparatus got results, and attracted the attention of other researchers. Many of the advances in analytical cytology from the 1940s and on-wards were made by people who made the pilgrimage to Stockholm. [Shapiro, 2004]

5.2.4 Laserscan microscopy

Laserscan microscopy (LSM) is a promising new imaging technique, as it has the capacity to detect low intensity light events. Furthermore, the better (x-, y-, z-) resolution over the classical light microscope and the reduced depth of field makes it very suitable for optical sectioning. Thus, if coupled with a digital image processing computer, LSM theoretically offers the possibility of 3 dimensional imaging of nuclei, in order to detect small clones of cells with a special function. Furthermore, in the near future systems to archive large image and knowledge data bases, together with intelligent statistical software, will become of help as expert (consultant) systems. [Baak, 1987]

5.2.5 Image cytometry

Image cytometry is the oldest form of cytometry. Image cytometers operate by statically imaging a large number of cells using optical microscopy. Prior to analysis, cells are commonly stained to enhance contrast or to detect specific molecules by labeling these with fluorochromes. Traditionally, cells are viewed within a hemocytometer to aid manual counting.

Since the introduction of the digital camera, in the mid-1990s, the automation level of image cytometers has steadily increased. This has led to the commercial

availability of automated image cytometers, ranging from simple cell counters to sophisticated high-content screening systems.

5.3 Hyperspectral Imaging

HSI technology acquires a 3-D image cube with two spatial dimensions and one spectral dimension in a noninvasive manner and in real time. Each pixel in the hypercube can be characterized by a spectral curve, which can range from UV to IR region. Spatially resolved spectra obtained by HSI provide diagnostic information about the tissue physiology, morphology, and composition. Furthermore, HSI can be easily adapted to other conventional techniques, such as microscopy, fundus camera, colposcopy, etc. As an emerging imaging technology, MHSI has been explored in a variety of laboratory experiments and clinical trials, which strongly suggested that HSI has a great potential for improving accuracy and reliability in disease detection, diagnosis, monitoring, and image-guided surgeries. Three major challenges confront the development and applications of HSI technology. The first challenge is the acquisition of high-resolution HSI datasets in video rates. Real-time acquisition will facilitate intraoperative imaging of the organs, tissues, cells, and molecular biomarkers of interest. Higher spectral and spatial resolution and a larger database of tissue spectra will provide more spatial and spectral information and may potentially capture more subtle spectral and spatial variations of different tissue types.

The second challenge involves the fast processing of the vast amount of datasets acquired by HSI, including the extraction of the high-quality diagnostic information, and generation of a quantitative map of different tissue types as well as diseasespecific endogenous substances. Advanced classification algorithms will enable better differentiation between healthy, premalignant, and malignant tissue, and more precise delineation of cancer margins for image-guided biopsy and surgery. Advanced spectral unmixing algorithms offer insight into the correlation between intrinsic biomarkers and disease states, and facilitate the identification of biomarkers for early cancer detection by recovering subpixel compositional information.

The third challenge lies in the establishment of a large spectra database for important molecular biomarkers and all types of tissue, including skin and subcutaneous tissue, ocular tissue, head/brain tissue, epithelial/mucous tissue, breast tissue, cartilage, liver, muscle, aorta, lung, myocardium, etc. Such a database will make it possible to distinguish not only between oxygenated and deoxygenated blood, but also between different tissue types, such as bile duct and the fatty tissue surrounding it. The identification of the molecular biomarkers can also benefit early cancer detection.

During the past two decades, HSI technology has undergone fast development in terms of hardware and systems, and has found numerous applications in medical domain. However, most MHSI only explores the UV, VIS, and NIR regions of light. Exploration of HSI on disease detection, diagnosis, and monitoring in the mid-IR region may bring new insights into the medical field. Moreover, combination with other imaging modalities, such as preoperative positron emission tomography and intraoperative ultrasound, can leverage the key benefits of each technique individually, overcome the penetration limitation of HSI into biological tissue, and broaden the application fields of HSI. In clinical settings, HSI can be easily adapted to conventional diagnostic tools, such as endoscope, colposcope, etc., to meet demanding requirements by various medical applications. Multimodal imaging combining reflectance and fluorescence has the potential of revealing more information about tissue under investigation. The clinical applicability of MHSI is clearly still in its adolescence and requires much more validation before it can be used safely and effectively in clinics. With the advancement of hardware technologies, image analysis methods, and computational power, we expect that HSI will play an important role for noninvasive disease diagnosis and monitoring, identification and quantitative analysis of cancer biomarkers, image-guided minimum invasive surgery, targeted drug delivery and tracking, and pharmaceutical drug dosage assessment.

Chapter 6

Conclusions

As we have already stated, the goal of this project is to create a brand new hyperspectral imager that combines the best features of all HSI types into a staring type machine. Indeed, we constructed a staring-type HSI with great throughput, high spatial resolution (6 MegaPixels), very high spectral resolution and no spatial scanning.

Our tomographic reconstruction process succeeded in reducing spectral deviation from $\pm 18.654\text{nm}$ to $\leq 1.3\text{nm}$. This figure will be re-validated in the future, while we implement spectral estimation algorithms instead of linear interpolation.

We believe that this work will shake the global industry's standards, as never before have we witnessed a staring hyperspectral imager with such high spectral resolution.

This work will also assist the medical industry, as our fluorescence microscopy systems, combined with our staring type HSI comprise a very powerful analytical tool for Quantitative Pathologists, Microbiologists, et al.

Bibliography

- Baak, J. (1987). "Quantitative Pathology Today - A Technical View". In:
- Balas, Costas (Nov. 2019). *Lecture in Beijing Institute of Technology*.
- Balas, Costas et al. (2018). "Hyperspectral Imaging and Spectral Classification for Pigment Identification and Mapping in Paintings by El Greco and his Workshop". In: URL: <https://link.springer.com/article/10.1007/s11042-017-5564-2>.
- Buhmeida, Abdelbaset (2006). "Quantitative Pathology: Historical Background, Clinical Research and Application of Nuclear Morphometry and DNA Image Cytometry". In:
- Collan, Y. et al. (1987). "Sampling in Diagnostic Morphometry: The Influence of Variation Sources". In:
- Fulwyler, M. J. (1965). "Electronic separation of biological cells by volume". In: DOI: [doi:10.1126/science.150.3698.910](https://doi.org/10.1126/science.150.3698.910).
- GmbH, Partec (2013). *Partec Flow Museum*.
- International Society for Advancement of Cytometry. URL: <https://web.archive.org/web/20130328203854/http://isac-net.org/ISAC-Cytometry/What-is-Cytometry.aspx>.
- Kong, S. G. et al. (2005). "Hyperspectral fluorescence image analysis for use in medical diagnostics". In:
- Li, Q. et al. (2012). "Nerve fibers identification based on molecular hyperspectral imaging technology". In: URL: <http://dx.doi.org/10.1186/1476-072X-11-21>.
- Lu, Guolan and Baowei Fei (Jan. 2014). *Medical hyperspectral imaging: a review*. URL: SPIEDigitalLibrary.org/jbo.
- Martin, R., B. Thies, and A. Gerstner (2012). "Hyperspectral hybrid method classification for detecting altered mucosa of the human larynx". In: URL: <http://dx.doi.org/10.1186/1476-072X-11-21>.

- Melgani, F. and L. Bruzzone (2004). "Classification of hyperspectral remote sensing images with support vector machines". In: URL: <http://dx.doi.org/10.1109/TGRS.2004.831865>.
- Monteiro, S. T. et al. (2004). "Towards applying hyperspectral imagery as an intra-operative visual aid tool". In: *Optical Filters by EdmundOptics*. URL: <https://www.edmundoptics.com/knowledge-center/application-notes/optics/optical-filters/>.
- Sack, U., A. Tárnok, and G. Rothe (2009). "Cytometry – a Definitive History of the Early Days". In:
- Shapiro, H. (2004). "The Evolution of Cytometers". In: DOI: [doi:10.1002/cyto.a.10111](https://doi.org/10.1002/cyto.a.10111).
- Sony IMX178. URL: <https://en.ids-imaging.com/sony-imx178.html>.
- Steinkamp, J. A (1973). "A new multiparameter separator for microscopic particles and biological cells". In: DOI: [doi:10.1038/171037b0](https://doi.org/10.1038/171037b0).
- Vojnovic, B. and P. Barber. *Spectral imaging applied to histology*. Gray Cancer Institute UK.